CERN/MPS/LIN. 71-2
August 1971

SPACE-CHARGE NEUTRALISATION OF INTENSE CHARGED PARTICLE BEAMS : SOME THEORETICAL CONSIDERATIONS

L.R. Evans, D.J. Warner

/fm

TABLE OF CONTENTS

SUMMARY

The problems treated in this report arose as a result of our experimental studies of the neutralisation of intense proton beams in the CERN 3 MeV linac. In the first section we present a formulation of the beam dynamics problem which we have used in the interpretation of our experimental data[1]. It enables us to calculate the maximum current for a beam of circular cross section which may be transmitted by a pair of separated circular apertures. It is demonstrated that the optimum beam is one of uniform current density and zero emittance. Next the potential distributions produced by ion beams inside typical metallic boundaries (often vacuum pipes) are studied. Essentially the Poisson equation has been solved numerically for cylindrical symmetry but with restricting apertures, stopping plates and variations in pipe diameter. All these geometries cause longitudinal electric field components. The influence of these fields on both the proton beam and on neutralising electrons is discussed.

Following this two models of space-charge neutralisation are proposed. The first treats the case of electrons created inside the beam potential well by ionisation of residual gas atoms. It is shown that for electrons of finite energy pulsed beams cannot be completely neutralised. A small potential well for electrons must still exist whose magnitude depends on the electron mean energy. A possible form of the potential distribution is calculated in a self consistent manner by assuming that the electrons are in thermal equilibrium.

The second neutralisation mechanism treated is that of secondary electron emission from the walls of the vacuum pipe or bounding electrode. It is shown that for a one-dimensional model the degree of neutralisation is governed by the space-charge limited electron current flowing from the walls into the beam.

Finally we discuss the effect of magnetic and electric fields on electrons produced by the two mechanisms treated above. It is demonstrated that even strong magnetic fields do not eliminate electrons which would be trapped in the beam in the absence of such fields. In addition it is shown that some electrons emitted from chamber walls which would not otherwise be trapped can nevertheless stay for relatively long times within the beam in the presence of quadrupolar magnetic fields. On the other hand, electric fields are effective in removing electrons from the beam.

1. INTRODUCTION

This paper can be considered complementary to our experimental study of space-charge neutralisation[1]. Limitations of space in Ref. 1) did not allow us to develop the theoretical and computational approaches we have used, so here we take the liberty of being more expansive. However, the theory and discussion presented here make no pretence of completeness; rather, the emphasis is on models which allow us to design and interpret experiments.

A few remarks are necessary on the limits we have put on our study. Throughout the paper we neglect the self magnetic field of the beam in comparison with the electric fields. For some problems the generalisation to include both effects is trivial - merely a factor $(1-\beta^2)$ in the terms involving radial forces, but as we refer our work mainly to 500 keV protons (where $\beta^2 \sim 10^{-3}$) we will rarely need to worry about such precision. Essentially then, our fields (electric) are determined as if the charges were static and Poisson's or Laplace's equations will apply.

We have not considered it useful to treat anything but cylindrical symmetry. This is sound with respect to the fixed apertures and beam pipes we have used in our experimental work but less justified for the beam real space sections and variable (rectilinear) apertures. However, it is an accepted procedure in low energy transport systems to maintain approximately

circular beam sections between successive triplets (to minimise space-charge induced emittance blow-up). In particular, for our optimised transmission experiments the circular section is normally dictated by circular defining apertures. Also, we have generally assumed that the increase in beam radius due to space charge (in un-neutralised beams) is much larger than that due to finite emittance.

Our third simplification is to use the constant current density beam as our standard of comparison. This is again related to the optimisation type of experiment.

In summary the philosophy used throughout has been to avoid generality if it seems to complicate unnecessarily the analysis or if anyway a specific point can be demonstrated adequately with zero emittance constant current density circular section beams.

2. RADIAL DYNAMICS OF ZERO EMITTANCE BEAMS WITH SPACE CHARGE

We base our treatment of the radial dynamics on the uniform density zero emittance beam. The now standard analysis[2] can be extended to two cases of interest to us : a) the computation of the maximum current transmitted by two separated circular apertures and b) a demonstration that the uniform density and zero emittance beam is the optimum beam in our transmission type experiments.

In brief, we have to solve the equation of motion

$$\ddot{r} = e E_r/m$$

which, for a proton beam of current I, radius r and velocity v gives as the equation for the beam envelope as a function of z :

$$\frac{d^2r}{dz^2} = \frac{1}{r} \cdot \frac{e I}{2\pi m v^3 \varepsilon_o} \quad . \qquad 2.1.$$

Integrating and putting $r = r_o$, $dr/dz = 0$ at $z = 0$ gives

$$\left(\frac{dr_z}{dz}\right)^2 = \frac{e\ I}{\pi m v^3 \varepsilon_o} \ln\left(\frac{r_z}{r_o}\right) , \qquad 2.2$$

$$= A^2\ I\ \ln(r_z/r_o) , \qquad \text{say}$$

hence

$$\frac{I^{\frac{1}{2}}\ A\ z}{2\ r_o} = \int_o^x e^{t^2}\ dt \qquad \text{with} \quad x = \left(\ln(r_z/r_o)\right)^{\frac{1}{2}} \qquad 2.3$$

The above result will be true for any radial distribution of current provided there is no ray crossing at the outer trajectories viz. if the proton which initially starts from r_o, 0 always stays the outermost proton in the beam. For an initially uniform density beam in which all proton velocities are directed parallel to the axis i.e. $dr/dz = 0$ at $z = 0$ for $0 \leq r \leq r_o$ there will be no ray crossing in the subsequent motion and the initial current density j_o scales with r_z thus $j_z = j_o\left(\frac{r_o}{r_z}\right)^2$ With any general current distribution $j(r)$, and $dr/dz = 0$ at $z = 0$ for $0 \leq r \leq r_o$ it is shown below that ray crossing will not occur as the beam grows at least until $r_z/r_o > 2.35$.

Consider the motion of a single particle starting with $r = s_o$, $dr/dz = 0$ at $z = 0$ just outside the beam treated above, viz. $s_o > r_o$. From 2.3

$$\frac{I^{\frac{1}{2}}\ A\ z}{2} = s_o \int_o^{x_s} e^{t^2}\ dt = r_o \int_o^{x_r} e^{t^2}\ dt . \qquad 2.4$$

If at some value of z, ray crossing occurs then $s_z = r_z$ and from our definition of x (eq. 2.3) :

$$s_o \exp(x_s^2) = r_o \exp(x_r^2)$$

We can now put 2.4 in Dawson's integral form :

$$\exp\ (-\ x_s^2) \int_o^{x_s} e^{t^2} dt \ = \ \exp\ (-\ x_r^2) \int_o^{x_r} e^{t^2} dt \ . \qquad 2.5$$

From tabulated values of Dawson's integral one sees that if $x_s > x_r$, equation 2.5 can only be satisfied for $x_r > 0.924$ i.e. $r_z/r_o > 2.35$. This result can be generalised to any ray in a beam of any current distribution because, until ray crossing occurs, all rays obey equation 2.3 with I corresponding to the current inside the radius of the trajectory under consideration.

2.1. Optimum Current Through Axially Separated Apertures

Consider two apertures, radii r_1 and r_2 separated by a distance ℓ. The maximum beam transmitted by the apertures will correspond to one of the possible beams which exactly passes through the apertures and comes to a waist ($r = r_o$) between the apertures. Applying (2.3) twice we obtain

$$I^{\frac{1}{2}} \ \frac{A}{2} \ (z_1+z_2) = \ r_o \int_o^{x_1} e^{t^2} dt + r_o \int_o^{x_2} e^{t^2} dt \ , \qquad 2.6$$

with

$$x_{1,2} = \left[\ln \left(\frac{r_{1,2}}{r_o} \right) \right]^{\frac{1}{2}} \ , \ z_1+z_2 = \ell$$

We require the value of r_o which corresponds to the maximum value of the r.h.s. of equation 2.6 and hence to the maximum transmitted current. For $r_1 = r_2$, 2.6 can be rewritten as :

$$\frac{AI^{\frac{1}{2}}\ell}{2r_1} = 2 \exp\ (-\ x_1^2) \int_o^{x_1} e^{t^2} dt \qquad 2.7$$

and, as above, we can use the tabulated values of Dawson's integral to show that the maximum value of the integral

$$D(x_1) = \exp(-x_1^2) \int_0^{x_1} e^t \, dt = 0.5410 , \qquad 2.8$$

which corresponds to $r_1/r_o = 2.349$.

We note that in the region of the maximum, the function $D(x_1)$ is very flat. In fact it is within 95% of its peak value for $1.7<r_1/r_o<3.9$. To find the optimum values for I and r_o when $r_1 \neq r_2$ we have used an iterative approach, obtaining results for 40 equally spaced values in the range $1<r_1/r_o<4.9$. A starting guess for r_o (= r_g) was derived from $(r_1 r_2)^{\frac{1}{2}}/r_g = C$ where C was the precise value of the ratio for the previous value of r_1/r_2 treated. The r.h.s. of 2.6 was calculated for three values 0.99 r_g, r_g and 1.01 r_g and by fitting a parabola to the results, optimum values of I and r_o were obtained (r_o always fell within the range of the three trial values).

A convenient way of expressing these results is by using the functions $F_1(r_1/r_2)$, $F_2(r_1/r_2)$ shown in Fig. 1, where :

$$F_1(r_1/r_2) = \frac{A^2 I_{max}}{4.685} \left(\frac{\ell^2}{r_1 r_2}\right) \quad * , \qquad 2.9$$

$$F_2(r_1/r_2) = \frac{r_o}{0.4257 (r_1 r_2)^{\frac{1}{2}}} . \qquad 2.10$$

In particular, for 510 keV protons,

$$I_{max} = 1313 \, F_1(r_1/r_2) \left(\frac{r_1 r_2}{\ell^2}\right) . \qquad 2.9a$$

It will be noted that the above analysis does not take into account image forces between the beam and the vacuum pipe. This means that the analysis is only strictly correct for circular beams inside circular pipes. Since in our experimental work the transport systems are all of circular symmetry and the proton beams are of nearly circular symmetry we neglect completely image foces in interpreting our experimental data.

---

* An error in equation (2) of Ref.1(b) corresponding to 2.9 above is given correctly in Ref. 1(a).

In the experimental work one invariably loses beam between the two defining apertures. These lost protons tend to reduce the possible optimum transmitted current as they contribute to the space charge repulsive forces in the early part of the motion but do not form part of the transmitted current. Our theory of optimum beams always assumes that all the current which passes through the first aperture also passes through the second and that the beam fills both apertures.

2.2. A Proof that Maximum Transmission Corresponds to the Uniform Zero Emittance Beam.

We demonstrate below that finite emittance and other than uniform current distribution will always tend to decrease the optimum current transmitted i.e. the case we have considered above corresponds to the maximum possible transmission.

Assume that a beam with arbitrary emittance and current density distribution (but circular symmetry) is 'optimised' so that maximum current I_m is transmitted by two apertures of radii r_1, r_2 separated by axial distance ℓ. Assume also that a beam waist of radius r_o occurs somewhere between the two apertures. Consider now the motion of a fictitious uniform density zero emittance beam, current I_m with waist r_o at the same position as for the general beam. Now we follow the outer trajectories of the fictitious and real beams towards say the aperture r_2. Clearly the envelopes of both beams will coincide until ray crossing of the outer trajectory occurs. Note that it is only a ray from the general beam which can cause cross-over. We compare the motion of the two beams from the point r_c, z_c at which there is ray crossing.

For the outer trajectories of both beams we have

$$\frac{d^2r}{dz^2} = \frac{A^2 I_m}{2r} \quad , \qquad 2.11$$

or

$$\frac{dr}{dz} = (A^2 I_m \ln r/r_c + c)^{\frac{1}{2}} \qquad 2.12$$

For the uniform beam let $dr/dz = B_c$ at r_c; for the general beam let $dr/dz = B_c(1 + \alpha)$ with α positive.

Hence for $r \geqslant r_c$

$$\frac{dr}{dz} = (A^2 I_m \ln r/r_c + B_c^2)^{\frac{1}{2}} \qquad 2.13a \text{ (uniform beam)}$$

or

$$\frac{dr}{dz} = \left(A^2 I_m \ln r/r_c + B_c^2 (1 + \alpha)\right)^{\frac{1}{2}} . \qquad 2.13b \text{ (general beam)}$$

Directly from 2.13a and 2.13b we see that at a given radius r the slope dr/dz for the general beam (with ray crossing) will be greater than for the uniform beam; at a given axial position $z > z_c$ this is equivalent to the radius of the general beam being larger than that of the uniform beam. Note that if, as is probable, further ray crossing occurs at the outside trajectory of the general beam then the previous argument continues to apply at the actual outer trajectory.

It follows that if ray crossing occurs the optimised general beam will have a larger radius at the defining aperture than the uniform beam. Hence one could obtain more current through the same aperture with a uniform beam. One could conceive of optimised beams with finite emittance and/or non-uniform current density where no ray crossing occurs at the outer trajectory between the apertures. The current, however, would not be greater than that of a uniform optimised beam. This then is the justification for using the uniform zero emittance beam to give the absolute upper limit for the current transmitted between a given pair of apertures.

Comparison of the results of beam transmission experiments with the optimum current derived above has proved to be a powerful technique for

detecting neutralisation in our beams. Often the upper limit given by 2.9a was substantially exceeded. In order to illustrate this effect, some typical experimental results are shown in Table 1, and are compared with the theoretical optima.

TABLE I

RESULTS OF TRANSMISSION EXPERIMENTS WITH 500 keV PROTON BEAM

l cm	r_1 cm	r_2 cm	Current in mA			Ratio
			I_{in}	I_{out}	I_{theory}	I_{out}/I_{th}
156	0.82	1.39	338	237	64	3.7
173	0.82	0.85	312	100	31	3.3
171	0.68	1.39	250	170	43	4.0
188	0.56	0.56	235	31	12	2.6

3. SPACE CHARGE POTENTIALS FOR BEAM WITH FINITE BOUNDARIES

In the previous section we have developed a formulation of the beam dynamics problem for an infinite cylindrical beam of uniform charge density inside an infinite cylindrical conducting pipe. In calculating the space-charge forces we have neglected the longitudinal variation of the beam envelope. Instead we have assumed that at each z-coordinate the beam may be replaced by an infinite cylindrical beam of the same radius.

In a low energy transport line there are often changes of beam diameter or vacuum pipe geometry over the length of the line. These changes invariably distort the ideal equipotentials and introduce longitudinal

field components. In this section we analyse the potential distributions in the presence of some boundary electrodes encountered in our practical work. In particular we are interested in the effect of aperture plates both biased and earthed, stopping plates or grids placed in the beam and abrupt changes in the pipe diameter.

There are several reasons for making these calculations :

i) In our experimental work we have observed that biasing a defining aperture at fairly low potentials (< 1 kV) produces a large decrease in the proton current measured later in the system. Therefore it is important to calculate the magnitude of any lens effects due to such apertures which may cause focusing of the proton beam. (One expects these effects to be small).

ii) The longitudinal fields introduced by changes in the beam or pipe geometry could have a much stronger effect on neutralising electrons present in the beam and could in this way influence the proton dynamics.

iii) During emittance measurements it is customary to place a metallic plate in the beam. This distorts the potentials and affects the motion of secondary electrons entering the beam from the plate. A study of these potentials when the plate is biased indicates the appropriate bias to use in order to eliminate the effect of these electrons.

As a standard for comparison we first treat the uniform cylindrical beam inside a cylindrical conducting pipe.

3.1. The Potential Distribution for an Infinite Cylindrical Beam in a Cylindrical Pipe

Consider an infinite cylindrical beam of radius 'a' and uniform charge density ρ inside a conducting pipe of radius r_p. The potential distribution for this case may be obtained by direct integration of the Poisson equation in free space with no longitudinal dependence

$$\text{i.e.} \quad \frac{1}{r}\frac{d}{dr}\left(r\frac{dV}{dr}\right) = -\frac{\rho}{\varepsilon_o} \qquad r \leqslant a, \qquad 3.1$$

$$= 0 \qquad a \leqslant r \leqslant r_p \quad .$$

Integrating these equations twice and matching the potentials and fields at the beam edge (r = a) gives

$$V(r) = \frac{I}{4\pi\,\varepsilon_o\,\beta c}\left(1 + 2\ln r_p/a - r^2/a^2\right) \qquad r \leqslant a\ , \qquad 3.2$$

$$= \frac{I}{2\pi\,\varepsilon_o\,\beta c}\ln\left(r_p/r\right) \qquad a \leqslant r \leqslant r_p\ .$$

Therefore the potential varies parabolically from the centre of the beam to the edge end thence logarithmically from the beam edge to the pipe. Here I is the beam current in amps and the other symbols have their usual meanings. It is useful to scale the potential V using as the unit of potential $I/(4\pi\varepsilon_o\beta c) = 30\ I/\beta$, which is the potential difference between the beam centre and edge. This gives approximately a scale for 500 keV protons ($\beta \sim .033$) of $\sim$.92 volts/mA.

The variation of potential with radius for $r_p = 2a$ is shown in Fig. 2, where we use the normalised radius $s = r/a$. One sees that the potential differences involved for the high current beams which exist in the low energy drift space of the CERN 3 MeV linac are quite large. For example, with a current of 500 mA and a vacuum pipe of twice the beam diameter the potential difference between the beam centre and the wall is $\sim$ 1.1 kV. Also, from equation 3.2 the potential between the pipe and axis varies with the ratio r_p/a. So if, for example, a focused beam decreases from a diameter $2r_p$ to a diameter r_p a longitudinal potential difference exists. For I = 500 mA this potential difference is $\sim$ 650 volts on the beam axis.

3.2. The Potential Distribution with Longitudinal Dependence

In this section we analyse the potential distributions for a number of bounding electrodes encountered in practice.

Poisson's equation for a cylindrically symmetrical beam is :

$$\frac{\partial^2 V}{\partial r^2} + \frac{1}{r}\frac{\partial V}{\partial r} + \frac{\partial^2 V}{\partial z^2} = -\frac{\rho}{\varepsilon_o} \qquad 3.3$$

It is again convenient to transform the potentials and distances to dimensionless coordinates $\eta = V(4\pi\ \varepsilon_o\ \beta c)/I$ and $s = r/a$, $z' = z/a$ thus

$$\frac{\partial^2 \eta}{\partial s^2} + \frac{1}{s}\frac{\partial \eta}{\partial s} + \frac{\partial^2 \eta}{\partial z'^2} = -4 \qquad 0 \leqslant s \leqslant 1$$

$$= 0 \qquad 1 \leqslant s \leqslant r_p/a \qquad 3.4$$

In general the solution of the Poisson equation with specified boundary conditions is sufficiently difficult mathematically to necessitate the use of numerical integration techniques, particularly when a large number of different cases must be treated. For this study, solutions have been found by the method of over-relaxation using a computer program developed by Hornsby[3]. The finite difference formulae used are those of the Poisson equation inside the beam boundary and Laplace outside. In order to match the solutions at the beam edge a special finite-difference approximation has been used (Appendix 1). Throughout we have used a square mesh of side, $h = 0.1$ units.

The accuracy of the numerical method was first tested by calculating the potentials for an infinite cylindrical beam inside an infinite conducting pipe - the analytical solution being given by equation 3.2. The numerical results are compared with 3.2 in Fig. 3 using two slightly different finite difference formulae at the beam edge (Appendix 1). We see for the better case that $\Delta\eta/\eta$ is always $< 0.22\%$. The computer program has been used to obtain solutions for a large number of different boundary conditions. Here we discuss some of the more important results which correspond to situations which are realised in our low energy transport line. The following features are common to all the computational results discussed.

i) The beam is assumed in all cases to be a uniformly charged cylinder of radius 'a' surrounded by an earthed conducting pipe normally of twice the beam diameter or, in some cases, equal to the beam diameter (e.g. apertures). We neglect the change in beam diameter and charge density due to the potentials.

ii) If a plate or aperture is biased it is separated from the pipe by a small distance over which the potential is assumed to vary linearly.

iii) Except for the case of a stopping plate the beam is assumed to extend to infinity in both positive and negative z directions. For computational purposes this is approximated by using a Neumann boundary condition $\partial\eta/\partial z' = 0$ at the vertical boundaries denoted by dotted lines in the diagrams. At these boundaries the radial potential distribution often approximates to that of the infinite beam. Some selected equipotentials are plotted and the positions and values of maximum or minimum potentials are recorded in parentheses.

In the following sections, potential plots for some selected geometries and bias values are discussed. Since we are interested in the motion of electrons in such fields we discuss the behaviour of a single 'test' electron which is normally trapped in the potential well created by the beam or, for a stopping plate, may enter the beam from the outside. We emphasise here that an interpretation of the behaviour of electrons is only correct when the electron density is sufficiently small not to perturb the potentials or when the electrons are distributed uniformly throughout the beam. The effect of the fields on the proton beam motion is discussed separately in 3.3.

3.2.1. *A Conducting Plate Perpendicular to the Beam*

This configuration is of particular interest because it approximates to the geometry during emittance measurements where a plate containing a narrow slit is placed in the beam. We assume that the slit is sufficiently narrow that the local perturbation of the potentials is small enough to

neglect its effect on the overall results. The potential plots in Fig. 4 a,b,c illustrate the solutions obtained for plate biases of +3, 0 and -3 units respectively. We see immediately that for zero and negative bias the plate potential always lies below that of the beam. Therefore the beam is always a sink for electrons. A 'test' electron trapped in the beam cannot be lost to the plate. Similarly an electron liberated from the plate is accelerated and focused into the beam and may be 'channelled' by the beam until it is deflected out of the potential well (e.g. by a magnetic field).

For positive bias the behaviour depends upon the magnitude of the bias. In Fig. 5 the axial potentials are plotted for a number of bias values both positive and negative. We see that the potential at the centre of the beam remains above that of the plate for potentials up to +2 units. Near the beam centre the direction of electron flow must still be from plate to beam although this may not be the case near the beam edge where the plate may be at the higher potential. In the plot for +3 units (Fig. 4a) the plate is everywhere at a higher potential than the beam. For this case no flow of electrons can occur from plate to beam. Similarly a 'test' electron in the beam can be lost to the plate if it is in a region where there is a longitudinal field. It follows that in order to prevent secondary electrons from entering the beam from the plate positive bias of at least 2 units should be used.

3.2.2. *Restricting Apertures*

This geometry is encountered during our 'optimisation' type experiments [1]. Here we are interested in the behaviour of electrons in the beam near the aperture and in the perturbation of the proton beam itself by the aperture.

Fig. 6 a,b,c correspond to aperture biases of +3, 0 and -3 units respectively. For the case of an earthed aperture the effect is to reduce the axial potential at the aperture by approximately 0.6 units. This corresponds to a potential barrier for a test electron trapped in the beam. It follows that for a beam with a restriction of this type the flow of

electrons between regions separated by the aperture is limited to those with sufficient energy to overcome the barrier. With negative polarisation this effect is accentuated; the potential barrier for electrons increases with increasing negative bias. This suggests that the flow of electrons between regions separated by a negatively biased aperture electrode could be considerably reduced. For positive bias the axial potential at the aperture approaches that of the electrode. In this case the behaviour of a test electron is governed by the magnitude of the bias. Axial potentials for a number of bias values are plotted in Fig. 7. We see that the beam potential barrier is gradually reduced until a well for electrons is established when the aperture electrode bias rises above about 2 units. The potential plot of Fig. 6a shows this effect for +3 units. Note that except for a small region outside the beam and close to the electrode, a test electron will not be attracted to the electrode but will oscillate in the potential well centred on the aperture. Considerably larger bias (4-5 units) is required to eliminate it from the beam.

3.2.3. *Changes in Vacuum Pipe Diameter*

A special type of aperture is that formed when the vacuum pipe diameter changes abruptly. Fig. 8 shows the potential distribution in the region of the junction when the pipe radius changes from 1 to 2 units. As expected from equation 3.2 a potential difference exists along the axis with the higher potential in the larger pipe. It follows that the flow of a 'test' electron along the beam is restricted to the direction from the smaller to larger pipe. Except for electrons with relatively large energy ($\sim$ 1 unit here), no such flow can occur in the reverse direction.

Finally we consider the structure shown in Fig. 9, which corresponds approximately to a drift tube/gap structure. From the symmetry of the system we see that this structure is equivalent to two pipes of unequal diameter with the Neumann condition applied much nearer the junction. The net effect is to reduce the axial potential difference considerably (only $\sim$ 10% of the two-pipe case). The potential distribution in the region of the beam depends very little on the radius of the outer boundary when it is more than about 1.5 times the gap distance.

3.3. Beam Focusing Effects Produced by Vacuum Pipe Discontinuities and Biased Electrodes

There were several reasons for studying focusing effects in our transport system which prompted us to go beyond the mere assertion that focusing effects were bound to be absolutely negligible for our 500 keV beam over the range of biases used ($\sim$ 2 kV).

i) In our transmission experiments the results were initially surprising to us. We have observed larger than expected transmitted currents (Table 1) which were very sensitive to bias on electrodes. Therefore it was necessary to consider the possibility of focusing effects.

ii) We were normally concerned with conditions at the edge of the beam (close to the electrode or aperture) where non-linearities argued against the use of paraxial equations. The methods which were developed to analyse and apply the results of our potential calculations could therefore be of more general interest.

We consider the beam to have constant radius in the region under analysis. Suppose one has an aperture electrode or other pipe discontinuity at z = 0. Then one can select limits z_{ℓ_1} , z_{ℓ_2} sufficiently far from the perturbed regions so that longitudinal field components can be neglected. In practice with our computed results z_ℓ will coincide with a Neumann boundary where $\frac{\partial \eta}{dz} = 0$ by definition.

From Gauss theorem :

$$\frac{\int_{z_{\ell_1}}^{z_{\ell_2}} E_r \, dz}{(z_{\ell_2} - z_{\ell_1})} = E_o \quad , \qquad 3.5$$

where E_r, E_o are measured at the same constant radius r within the beam, E_o being the normal unperturbed radial field (see Fig. 10).

Relative to the normal space charge defocusing (typified by E_o) there is only a second order focusing effect which we consider is produced by several lens actions of alternating sign. For example, the unbiased aperture can be analysed as an FDF triplet according to the way E_r changes with z (Fig. 10).

From each of the potential plots treated in the previous section one determines the values of $(E_r - E_o)$ at r = 0.9 a (to avoid the infinity in E_r one often has at r = a) via the potential differences between the points at r = 0.8 a, r = a respectively. E_o on this scale is 1.8 V_o/a where V_o is the unperturbed potential difference between the centre and the beam edge. To within the accuracy required one obtains by simple summation the integrals

$$I_n = \int_{z_n}^{z_{n+1}} (E_r - E_o)\, dz \qquad 3.6$$

where z_n, z_{n+1} are limits to a region in which values of the argument have the same sign; this gives two independent estimates to be used to calculate the lens strengths (in a two element system). It is not difficult to locate the ends of the effective lens and its median position $\bar{z}_n$ defined as :

$$\int_{z_n}^{\bar{z}_n} (E_r - E_o)\, dz = \int_{\bar{z}_n}^{z_{n+1}} (E_r - E_o)\, dz \quad . \qquad 3.7$$

To calculate the effective lens strength at r = 0.9a we use

$$\delta_n = \frac{1}{f} = \frac{1}{0.9\ a} \cdot \frac{\tfrac{1}{2}\, e \int_{z_n}^{z_{n+1}} (E_r - E_o)\, dz}{\tfrac{1}{2}\, m\, v^2} \quad . \qquad 3.8$$

From equation 3.5 we note that the total negative and total positive integrals should be equal in magnitude; one must use exactly equal values to calculate the values of δ. However, $\frac{1}{2}\,mv^2$ will generally be different for δ_n, δ_{n+1}. With $\frac{1}{2}\,mv^2 = e(V_{inj} - \Delta V_n)$, then V_{inj} = 500 kV and ΔV_n is an average value between z_n, z_{n+1} for the plotted potential at r = 0.9 a. (ΔV_n at the lens median position $\bar{z}_n$ is usually good enough). Thus one can express the lens power as

$$\delta_n = \frac{I_n}{1.8\ a}\ \frac{1}{V_{inj}} \cdot \left\{ 1 + \frac{\Delta V_n}{V_{inj}} \right\} \quad . \qquad 3.8(a)$$

The overall strength of our alternating lens system is given by :

$$\delta_{eff} = (1 + \delta_2 \ell)\ (2\delta_2 + \delta_1 + \delta_1 \delta_2 \ell)\ , \qquad 3.9(a)$$

Symmetric triplet

$$\delta_{eff} = \delta_1 + \delta_2 + \delta_1 \delta_2 \ell \qquad 3.9(b)$$

Doublet

for assumed linear point lenses of strengths δ_1, δ_2 separated by a distance ℓ . The sum term $(2\delta_2 + \delta_1)$ can be up to $\sim$ 5 times as large as the product term $\delta_1 \delta_2 \ell$ in the cases we have considered (Table 2). The error in equation 3.8 for δ_n in that the change of charge density with v has been neglected could thus be important e.g. the sum term could in the most pessimistic view be only 2/3 of its correct value. To retain a simple formalism we do not attempt to correct for this error which normally is largely compensated by the way we obtain ΔV_n. Table 2 summarises the results obtained with different geometries and biases and compares the focusing strengths with the defocusing of the beam space charge over the same distance, where the self defocusing strength is

$$\delta_s = \frac{\ell_s}{a^2}\ \frac{V_o}{V_{inj}} \quad , \qquad 3.10$$

where ℓ_s is the length between the outermost elements of the lens system.

TABLE II

FOCUSING EFFECT OF BIASED ELECTRODES AND PIPE DISCONTINUITIES

Electrode Type	Figure No.	Bias/V_o	I_2/V_o	$\frac{(\Delta V_2 - \Delta V_1)}{V_o}$	ℓ/a	$\frac{2\delta_2+\delta_1}{\delta_1\delta_2\ell}$	δ_{eff} m^{-1}	δ_s m^{-1}
Aperture	6(b)	0.0	- 0.24	0.82	1.20	5.1	22.10^{-6}	12.10^{-2}
Aperture	6(c)	- 3.0	- 0.82	2.83	1.42	4.4	268.10^{-6}	14.10^{-2}
Aperture	6(a)	+ 3.0	+ 0.32	- 1.15	1.60	4.0	43.10^{-6}	16.10^{-2}
Pipe (i) Discontinuity	8	0	- 0.38	0.86	1.20	see (i)	20.10^{-6}	6.10^{-2}
'Structure'	9	0	+ 0.19	- 0.33	0.74	4.1	8.10^{-6}	8.10^{-2}

Notes (i) All cases except the pipe discontinuity are treated as triplet lenses with I_2, δ_2 corresponding to the outer element. Ratio $(\delta_2+\delta_1)/\delta_1\delta_2\ell = 3.4$ for pipe discontinuity.

(ii) Values of δ_{eff} , δ_s are given for 500 mA proton beam, a = 0.01 m, V_{inj} = 500 kV (V_o = 459 V).

A more detailed analysis using empirical functions for the potentials and radial fields at r = 0.9 a for the unbiased aperture is given in Appendix 2.

One important case that we do not need to treat by this method corresponds to the special apparatus used in our experimental work[1]. The alternate positive and negative biases on the cylindrical electrodes correspond to a series of lenses each with focal length given by [8]

$$\frac{1}{f} = \left(\frac{\Delta V}{2V_{inj}}\right)^2 \cdot \frac{1.315}{4\ a} \quad . \qquad 3.11$$

For a = 1 cm, ΔV = 1 kV then $1/f = 33.10^{-6}\ m^{-1}$ compared with $\delta_s = 9.10^{-2}\ m^{-1}$ for I = 200 mA.

Thus we may conclude from the results in Table 2 and the above result for cylindrical lenses that all focusing effects produced during our experiments by applied bias or self-induced field perturbations can be neglected.

4. THEORETICAL MODELS OF SPACE CHARGE NEUTRALISATION

In the present section two possible mechanisms for neutralisation are discussed. The first treats the case of electrons created within the beam potential well by ionisation of residual gas atoms while the second deals with the alternative mechanism of neutralisation by secondary electron emission from the metallic walls of the vacuum pipe.

4.1. Gas Neutralisation

It has long been known that space charge neutralisation by ionisation of residual gas is an important factor in high current C.W. electron beam devices [4]. In order that this mechanism be effective for pulsed proton beams the gas pressure must be sufficiently high that the required electron concentration is attained in a time τ which is short compared with the beam pulse duration.

The rate of production of electrons per unit volume by the bombardment of gas atoms of concentration N_g by a proton flux $\phi(cm^{-2}.sec^{-1})$ is :

$$R_i = \phi \Sigma N_g \quad , \qquad 4.1$$

where Σ is the total ionisation cross section appropriate to the proton energy and gas species. For molecular hydrogen, which is the principal gas in the low energy drift space of the 3 MeV Linac, and for 500 keV protons, $\Sigma \sim 5.10^{-17}\ cms^2$. The time τ for the electron density to equal

the proton density ϕ/v_p assuming no electrons are lost is then given by

$$\tau = \left(N_g \Sigma v_p \right)^{-1} \quad , \qquad 4.2$$

where v_p is the proton velocity. For the low energy drift space of the 3 MeV Linac, where the gas pressure is typically $\sim 2.10^{-4}$ torr we get $\tau \sim 3$ μsec. Therefore for most of our 20 μsec proton beam pulse it may be possible for a considerable degree of neutralisation to occur provided all created electrons are trapped. In practice electrons are produced with a distribution of energies and only those with energy less than a certain value (depending on their point of creation) will be trapped. In the following section the energy distribution of ejected electrons is calculated and their effect on the simple model is discussed.

4.1.1. *The Energy Distribution of Electrons Produced by Collisional Ionisation*

The energy distribution of electrons produced by ionising collisions may be calculated with the aid of a classical model developed by Gryzinski[5] (an algebraic error in the Gryzinski paper has been corrected in Ref. 6)). Here the cross section $\sigma(\Delta E)$ for an energy transfer E between a proton and a free electron is calculated from the Coulomb forces between proton and electron, and is given by :

$$\sigma(\Delta E) = \left(\frac{2\pi e^4}{m_1 v_2^2} \right) \cdot \left(\frac{v_2^2}{v_1^2 + v_2^2} \right)^{3/2} \cdot \frac{1}{(\Delta E)^2}$$

$$\times \begin{cases} 1 + \frac{4}{3} \frac{E_1}{\Delta E} & \Delta E \leq K_{12} E_2 (1 - v_1/v_2) \\ \frac{1}{2}\left[\left(1 + \frac{\Delta E}{E_1}\right)\left(\frac{1}{3} + \frac{4}{3}\frac{E_1}{\Delta E}\right) + 1 + \frac{4}{3}\frac{E_1}{\Delta E} - \frac{1}{6}\frac{v_1}{v_2}\frac{(\Delta E)^2}{K_{12} E_1 E_2} \right] & \Delta E \geq K_{12} E_2 (1 - v_1/v_2) \end{cases} \qquad 4.3$$

where m_1, m_2, v_1, v_2 are the electron and proton masses and velocities respectively, E_1 and E_2 their energies and $K_{12} = 4 m_1 m_2/(m_1 + m_2)^2$

Equation 4.3 was derived on the basis of two body collisions between free particles. However, it has been shown that the equation gives reasonable results for a target electron which is bound provided that the energy transfer is greater than the ionisation potential U_i. Then for molecular hydrogen, $E_1 = U_i = 15.6$ eV, $v_1 = (2e\ U_i/m_1)^{\frac{1}{2}}$ and the cross section in 4.3 must be doubled to take into account the effect of both electrons. The differential cross section $\sigma(E)$ for the production of free electrons with energy $E = \Delta E - U_i$ is shown in Fig. 11. This curve is also proportional to the density of electrons per unit energy range 'n_e' since

$$n_e\ dE = \phi\ N_g\ \sigma(E)\ dE \quad , \qquad 4.4$$

where ϕ is the proton flux.

The fraction F(E) of these electrons with energy less than E is given by

$$F(E) = \int_o^E \sigma(E)\ dE \Big/ \Sigma \quad , \qquad 4.5$$

where Σ is the total cross section used in 4.1 and is

$$\Sigma = \int_o^{\Delta E_{max} - U_i} \sigma(E)\ dE \quad , \qquad 4.6$$

ΔE_{max} is the maximum energy lost by the proton and is

$$\Delta E_{max} \simeq K_{12} E_2 (1 + v_1/v_2) \quad . \qquad 4.7$$

From Fig. 12 we see immediately that the time for complete neutralisation estimated in equation 4.2 is optimistic. For example, suppose that the beam is neutralised until the potential well depth is V_R volts. We may calculate approximately the time required by assuming that all electrons with an energy greater than V_R are lost. The curve in Fig. 13 shows this

time normalised to the time τ in 4.2 which assumes implicitly that all electrons are produced with zero energy. The error bars reflect the uncertainty in calculating the number of trapped electrons due to the spatial variation of potential within the beam. One sees that the time required to achieve complete neutralisation is infinite. Therefore our pulsed beams cannot be completely neutralised in this way. A potential well for electrons must exist (the depth of which decrease with time) of sufficient magnitude to trap electrons.

Note that for heavy ions of atomic weight A, charge Z and with the same energy E_2 as for the proton case above, the total cross section is increased in the ratio

$$\Sigma_A/\Sigma = Z\,A\left[\frac{v_A^2}{v_A^2 + v_1^2}\right]^{3/2} \qquad 4.8$$

$$\simeq Z\,A \quad \text{for } Z\,A \lesssim 200 \,.$$

The neutralisation time τ calculated in 4.4 is correspondingly reduced in the ratio

$$\tau_A/\tau = 1/\sqrt{Z\,A} \,. \qquad 4.9$$

A self consistent description of the potential distribution in the presence of neutralisation is rendered difficult because of the complicated distribution of electrons in the beam and in the space between beam and pipe. These difficulties may be overcome if one assumes a model for the neutralised beam in which the electrons are in thermal equilibirum with themselves i.e. the steady state distribution is determined completely by electron-electron Coulomb collisions and is independent of the kinetic and potential energies of electrons at their point of production. This model is only applicable when the rate of production is slow compared with the thermalisation time t_R given by [7]

$$t_R = \frac{0.26\ T_e^{3/2}}{n_e \ln \Lambda} \,. \qquad 4.10$$

Here n_e and T_e are the equilibrium electron density and temperature (in ^oK) and $\ln \Lambda$ is a factor which represents the shielding of the Coulomb fields and is generally between 5 and 20 depending on n_e and T_e. Using this formula one finds that for electrons of mean energy 10 eV (1 eV) i.e. $T_e = 1.2 \times 10^5$ $(1.2 \times 10^4)^oK$, $n_e \sim 10^9$ cm^{-3} then $t_R \sim 600$ μsec (25 μsec) respectively. Therefore this model applies to long beam pulse duration (tending to d.c.) and low gas pressure ($\lesssim 10^{-6}$ torr). Since this model is not of direct interest to us because our experimental conditions are far from its range of validity it is not developed here but is discussed in Appendix 3.

4.2. Neutralisation by Secondary Electron Emission

As part of our experimental work we have studied the behaviour of proton beams passing through the Alvarez cavity of the 3 MeV Linac without acceleration or external focusing. It was shown that even though the gas pressure was too low for sufficient production of electrons by gas ionisation the beam was still highly neutralised. In order to explain these results we have proposed that the neutralising electrons are produced by secondary emission from the walls of the drift tubes. In support of this mechanism it was shown experimentally[1] that the secondary emission coefficient for proton impact at glancing incidence is much greater than at normal incidence ($\sim$ 30 for incidence of 1^o, compared with 2 for normal incidence). Therefore even though these electrons are not trapped they flow continuously across the beam in sufficient numbers to cause neutralisation provided enough beam loss occurs. In the present section a simple one-dimensional model of this mechanism is derived. It is shown that the beam cannot be completely neutralised but the flux of electrons into the beam is governed by the space charge limited electron current from the walls.

Consider an infinite proton beam of uniform density ρ_+ bounded by a pair of infinite plane parallel conducting plates at $\pm a$ and at a potential V_a relative to the beam centre. Assume that a uniform flux j_-

of electrons is liberated with zero initial velocity from each plate.

Then the charge density ρ_- of electrons at any point x where the potential is V(x) is given by :

$$\rho_- (x) = 2j_- \left(2e(V(x) - V_a)/ m\right)^{-\frac{1}{2}} \qquad 4.11$$

The potential distribution in the beam is then given by the Poisson equation in one dimension i.e.

$$\frac{d^2V}{dx^2} = \frac{1}{\varepsilon_o}\left[\rho_+ - 2j_-\left(\frac{m}{2e(V_a - V(x))}\right)^{\frac{1}{2}}\right] \qquad 4.12$$

where we replace V by - V for convenience.

A first integration of this equation using the symmetry condition dV/dx = 0 at x = 0, V = 0 gives

$$\left(\frac{dV}{dx}\right)^2 = \frac{2}{\varepsilon_o}\left[\rho_+ V + 4j_-\left(\frac{m}{2e}\right)^{\frac{1}{2}}\left[\left(V_a - V(x)\right)^{\frac{1}{2}} - V_a^{\frac{1}{2}}\right]\right] . \qquad 4.13$$

Now the maximum value that j_- can have which makes the right hand side of 4.13 positive over the whole range $0 \leqslant V(x) \leqslant V_a$ is :

$$j_{max} = \frac{\rho_+}{4}\left(\frac{2e\ V_a}{m}\right)^{\frac{1}{2}} . \qquad 4.14$$

This, then is the maximum current density of electrons which can be injected into the beam. This is analogous to the well-known Child-Langmuir law for space charge limited current flow in a planar diode. For $j_- = j_{max}$ the field at the plates reduces to zero.

Equation 4.13 can be conveniently reduced to dimensionless form by putting $\eta = V/V_o$, where $V_o = \rho_+ a^2/2\varepsilon_o$, (the potential difference between the centre and edge of the beam in the absence of neutralisation), $s = x/a$ and $f = j_-/j_{max}$ giving :

$$\left(\frac{d\eta}{ds}\right)^2 = 4\left\{ f\left(\eta_a \ (\eta_a - \eta)\right)^{\frac{1}{2}} - (f\eta_a - \eta) \right\} \qquad 4.15$$

The general solution of 4.15 for $0 \leqslant s \leqslant 1$ is then

$$s = \eta_a^{\frac{1}{2}}\left[\frac{f\pi}{4} + \left(1 - f + f\left(1 - \eta/\eta_a\right)^{\frac{1}{2}} - \left(1 - \eta/\eta_a\right)\right)^{\frac{1}{2}} - \frac{f}{2}\sin^{-1}\left[\frac{2\left(1 - \eta/\eta_a\right)^{\frac{1}{2}} - f}{2 - f}\right]\right]$$

with $s = 1$ at $\eta = \eta_a = V_a/V_o$. 4.16

Fig. 14 shows the variation of η with s given by this equation for f = 0, 0.5 and 1. We see that on this model it is impossible to reduce the potential well to less than $\sim$ 40% of its original value. It can be shown that for the limiting case the total number of electrons inside the beam is equal to the total number of ions (as required by Gauss theorem for $d\eta/ds = 0$ at $s = 1$) but with a large electron concentration (in fact a singularity) at the beam edge.

We have been unable to extend this analysis to beams with cylindrical symmetry due to the difficulty of a singularity in charge density at the beam centre unless one presupposes some angular and velocity distribution of ejected electrons. However, one would expect the same relationship between this case and the space charge limited current in a cylindrical diode as we have noted for the planar geometry relative to the planar diode.

5. THE EFFECT OF MAGNETIC FIELDS ON NEUTRALISATION

In most low energy transport lines there exist a number of magnetic focusing elements. In the low energy drift space of the 3 MeV Linac for example, there are two sets of quadrupole triplet lenses. In this section we discuss the effect of such fields on the motion of neutralising electrons.

5.1. The Effect on Trapped Electrons

The model developed in 4.1.1 predicts that a pulsed beam cannot be completely neutralised by gas ionisation but that some small potential well must exist in which electrons are trapped. These trapped electrons cannot be directly eliminated from the beam by magnetic fields of any configuration or strength since these fields can impart no energy to the electrons which will enable them to leave the potential well. Their orbits in such fields may be extremely complicated. Here for simplicity we consider only electrons in the defocusing plane of a quadrupole lens; the treatment in the focusing plane involves essentially only a sign change.

It can be shown[7] that in the presence of a non-uniform magnetic field an electron moves in quasi circular orbits at the cyclotron frequency such that there is a drift of the centre of gyration with the drift velocity given approximately by

$$v_d = \tfrac{1}{2}\, mv^2 \cdot \frac{\nabla B}{eB^2} \quad . \qquad 5.1$$

For a quadrupole field of gradient G this then becomes

$$v_d = \frac{2.85 \times 10^{-12}\, v^2}{Gx^2} \quad , \qquad 5.1(a)$$

where the velocities are in $m.sec^{-1}$, G is in Tesla m^{-1} and x is the distance of the centre of gyration of the electron from the quadrupole axis in metres.

In the presence of a radial electric field an additional drift motion is introduced due to the crossed electric and magnetic fields. If we neglect the magnetic field gradient and assume that at any point the magnetic field is uniform and of strength B we get for this drift :

$$v_e = E/B \quad , \qquad 5.2$$

or assuming a linear electric field E = kx

$$v_e = k/G. \qquad 5.2(a)$$

For electrons both the drifts of 5.1 and 5.2 are in the same sense.

We see that the drift motion 5.2 is independent of the position x of the centre of gyration and decreases with increasing magnetic field gradient. In order to investigate the motion of electrons in the presence of both E and ∇B fields the equations of motion are solved numerically. In Cartesian coordinates they are :

$$\begin{aligned} \ddot{x} &= -\left[E_x - \dot{z}\, Gx\right] . e/m \ , \\ \ddot{y} &= -\left[E_y + \dot{z}\, Gy\right] . e/m \ , \qquad 5.3 \\ \ddot{z} &= -\left[\dot{x}\, Gx - \dot{y}\, Gy\right] . e/m \ , \end{aligned}$$

where

$$E_x = kx, \quad E_y = ky \quad \text{for } (x^2 + y^2)^{\frac{1}{2}} < a$$

$$E_x = \frac{ka^2x}{x^2+y^2} \ , \quad E_y = \frac{ka^2y}{x^2+y^2} \quad \text{for } (x^2 + y^2)^{\frac{1}{2}} > a$$

and $k = I/(2\pi\, \varepsilon_o\, \beta\, ca^2)$.

This set of 3 simultaneous second order differential equations may be reduced to 6 first order equations which may then be solved by Runge Kutta integration.

Some typical results are shown in Fig. 15a and b for an electron of 20 eV. In Fig. 15a the electric field has been removed so that the motion corresponds to that given by the approximate equation 5.1 and is compared with the analytical result (dotted) for the position of the centre of gyration at the end of the computation (25 nsec). Fig. 15b shows the corresponding motion including an electric field due to a residual space

charge of a current of 20 mA. We see here that the drift velocity has increased but is still considerably lower than that in the absence of magnetic fields ($\sim$ 6.7 cms drift in 25 nsec.).

Within the limitations of the above analysis we have shown for focusing and defocusing planes the type of motion expected. However we cannot claim to have developed a self consistent treatment for a high degree of neutralisation when the distribution with azimuth of electrons could modify the field configuration considerably.

5.2. The Effect on Electrons Produced from the Walls

As stated in 4.2, we have observed neutralised beams in regions where the most probable neutralisation mechanism is secondary electron emission from the metallic walls of the beam channel (the drift tubes of the Alvarez cavity in our case). One might expect that these electrons could quickly be eliminated from the beam by using the quadrupole lenses in the drift tubes. When this was attempted experimentally it was found that the effect observed was much less than expected.

In order to explain this result the motion of electrons liberated from the wall of a drift tube have been computed again using equations 5.3. These results show that in certain regions of the quadrupole where the magnetic field is nearly radial, electrons can be effectively trapped for times much larger than their unperturbed transit time across the drift tube bore. In order to illustrate this effect, Fig. 16 shows an orbit of a typical electron which exhibits this behaviour. The regions in which this effect may occur are restricted to about 10^{o} in each quadrant of the lens, so that only about 10% of the secondary electrons are 'trapped'. Even so, it seems that they must still be effective in maintaining a neutralised beam, for example the computation illustrated in Fig. 16 has been arbitrarily stopped after 100 nsec.

6. EFFECT OF ELECTRIC FIELDS ON NEUTRALISATION

In our experimental work we have seen the effect of biased apertures on beams and have intentionally used a series of biased electrodes to remove electrons from the beam over a metre distance. The manner in which biased electrodes act is not completely trivial in the presence of space charge; as we saw in section 3.2.2. a potential well for electrons within the beam still exists in the presence of substantial positive bias (see Fig. 6a). In order to achieve complete elimination of electrons from the beam, i.e. for the collecting electrodes to be at the highest potential in the system, one needs for the biased aperture case, $\sim$ 4-5 units which is $\sim$2 kV for a 500 mA, 500 keV proton beam. However electron elimination from a partially neutralised beam starts at much lower biases and will proceed with increasing bias until an unneutralised beam is obtained. An experimental curve which can be interpreted as a gradual transition from partially neutralised towards an unneutralised beam is given in Fig. 3 of Ref. 1.

7. CONCLUSIONS

The topics presented here were of interest in helping our understanding of some of our experimental work on neutralised beams. The emphasis has been on the treatment of the simplest relevant cases so there are some obvious refinements and extensions possible in the direction of finite emittance, non-circular symmetry, non uniform density distribution and bunched beams. Some unsatisfactory features are apparent in the models for neutralised beams particularly as regards the transient or equilibrium states; a self consistent model is desirable. However it is clear that beam dynamics calculations made neglecting neutralisation cannot be generalised rigorously to partially neutralised beams simply by the introduction of a global neutralisation factor((1 - f) in the literature) into the computation of the radial space charge field.

In view of the difficulties in understanding and hence controlling neutralisation we would suggest that the design of focusing channels for intense low energy proton beams (e.g. at 500 keV for the CERN 50 MeV and 3 MeV linacs) should not rely on this type of self neutralisation. Instead the design should be made with sufficient lenses to ensure that emittance effects are predominant over space charge effects in determining the proton dynamics.

It is worth repeating here that one should apply with caution the results of dynamics computations to practical systems in which neutralisation could occur.

ACKNOWLEDGEMENTS

We would like to thank C.D. Johnson for helpful discussion concerning ionisation cross sections.

REFERENCES (Including appendices)

1) L.R. Evans, D.J. Warner. Studies of Space Charge Neutralisation in Intense 500 keV Proton Beams.a)IEEE Trans. Nucl. Sci. NS-18, No. 3, 1068 (1971). b)CERN Internal Report CERN/MPS/LIN 71-3.

2) J.R. Pierce. Theory and Design of Electron Beams. Van Nostrand, London, (1954).

3) J.S. Hornsby. A Computer Program for the Solution of Elliptic Partial Differential Equations. CERN Yellow Report 63-7 (1963).

4) L.M. Field, K. Spangenberg, R. Helm. Control of Electron Beam Dispersion at High Vacuum by Ions. Elec. Communication, 24, 108 (1947).

5) M. Gryzinski. Classical Theory of Electronic and Ionic Inelastic Collisions. Phys. Rev., 115, 374 (1959).

6) R.G. Allsmiller. Dissociation and Ionisation of H_2^+ by Electrons and Protons. ORNL Report ORNL-3232 (1962).

7) L. Spitzer. Physics of Fully Ionised Gases. Interscience, New York, (1956).

8) D.H. Menzel (ed.). Fundamental Formulas of Physics. Vol. 2,441 (Dover N.Y. 1960).

Distribution (open)

Abstract sent to ISR, MPS and SI Scientific Staff

APPENDIX 1

THE FINITE DIFFERENCE EQUATIONS AT A POISSON/LAPLACE INTERFACE

In the two regions of Fig. Ap.1 the equations(3.4) apply viz :

$$\frac{\partial^2\eta}{\partial s^2} + \frac{1}{s}\frac{\partial\eta}{\partial s} + \frac{\partial^2\eta}{\partial z'^2} = -4 \qquad s \leqslant 1$$

$$= 0 \qquad s \geqslant 1$$

Essentially we have to derive a finite difference equation for point 8 involving $\eta_5, \eta_7, \eta_8, \eta_9$ and η_{11} only, given 7 equations involving $\eta_1, \eta_2, .., \eta_{15}$.

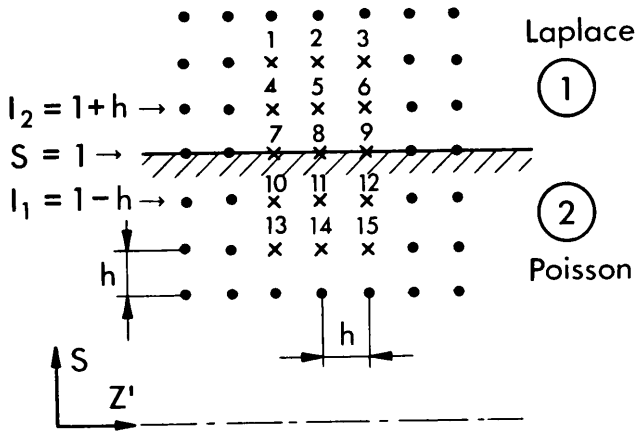

Fig. Ap. 1

The following equations invoke the continuity of $\frac{\partial\eta}{\partial s}$ at s = 1 :

$$2h \left.\frac{\partial\eta}{\partial s}\right|_i \tilde{=} 4\eta_{i-3} - 3\eta_i - \eta_{i-6} = 3\eta_i + \eta_{i+6} - 4\eta_{i+3} \qquad \text{(i)}$$

which applies for i = 7, 8 and 9 respectively.

Finite difference forms of the Poisson/Laplace equation in each region can be stated in normal and diagonal form :

Normal Form : $$\eta_{i+1} + \eta_{i-1} + a_i\eta_{i-3} + b_i\eta_{i+3} - 4\eta_i = -\rho_i \quad , \qquad \text{(ii)}$$

Diagonal Form : $$a_i(\eta_{i-4} + \eta_{i-2}) + b_i(\eta_{i+2} + \eta_{i+4}) - 4\eta_i = -2\rho_i \quad . \qquad \text{(iii)}$$

The equations apply at i = 5 and 11 respectively with

$$a_5 = 1 + h/2I_2 \quad , \quad b_5 = 1 - h/2I_2 \quad , \quad \rho_5 = 0 \quad ,$$

$$a_{11} = 1 + h/2I_1 \quad , \quad b_{11} = 1 - h/2I_1 \quad , \quad \rho_{11} = -4h^2 \quad .$$

The elimination of the unwanted η_k poses little problem except for the combination $(a_5\eta_2 + b_{11}\eta_{14})$ for which one uses the approximation

$$a_5\eta_2 + b_{11}\eta_{14} = \eta_2+\eta_{14}+(2\eta_5-\eta_8)h/2I_2 - (2\eta_{11}-\eta_8)h/2I_1 \quad . \tag{iv}$$

Finally one obtains (neglecting terms of order h^2)

$$\eta_5\left(1 + 0.5\ h\right) + \eta_{11}\left(1 - 0.5\ h\right) + \eta_7+\eta_9-4\eta_8 = -\ 2h^2\left(1 - 0.5\ h\right). \tag{v}$$

One expects the relation (v) from the argument that as the area bounded by 9,5,7 and 11 falls half in each region then $-\ 2h^2$ (instead of $-\ 4h^2$) would be the natural value to choose. The small correction (h/2) results from the circular symmetry. In Fig. 3 the comparison of numerical results using $-\ 2h^2$ and $-\ 2h^2(1 - .5h)$ respectively with the theoretical result (eq. 3.2) favours $-\ 2h^2$ mainly because the finite difference approximation in the Laplace region also leads to comparable errors. In fact we have used $-\ 2h^2$ throughout our computations.

Consider two particular cases where the boundary does not pass through mesh points. In Fig. Ap . 2, on our basic mesh points 1,5,7,9 and 13 we have superimposed a half size mesh such that the boundary now passes through 2,3 and 4. For simplicity one develops six equations in a two dimensional system of type :

$$\eta_i+\eta_j+\eta_k+\eta_\ell-4\eta_m = -\ \rho_n \quad . \tag{vi}$$

These can be reduced to :

$$\eta_1+\eta_5+\eta_9+\eta_{13}-4\eta_7 = -\ 3.5\ h^2 \quad . \tag{vii}$$

This is the expected result as square 1,5,13,9 has $\frac{7}{8}$ of its area in the Poisson region. Similarly when the boundary passes through 10, 11 and 12 the charge term is $-\ 0.5\ h^2$.

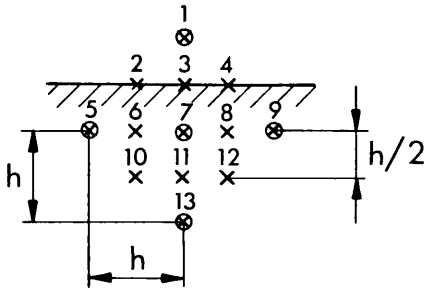

Fig. Ap. 2

APPENDIX 2

FOCUSING EFFECT OF APERTURE - AN ANALYTICAL SOLUTION

In section 3.3 we have given a procedure for estimating the focusing effects of beam pipe discontinuities on the proton beam without considering the detailed form of the functions $E_r(z)$, $\Delta V(z)$. For the zero bias aperture (Fig. 6b) there is a reasonable fit at r = 0.9 a to

$$(E_r - E_o) = \Delta E(z) = \Delta E(o)\, \exp(-b|z|)\left(1 - b|z|\right), \qquad \text{(i)}$$

$$\Delta V(z) = -\Delta V(o)\, \exp(-.5b|z|). \qquad \text{(ii)}$$

The use of $|z|$ ensures symmetry about z = 0 and E_r of eq. (i) satisfies eq. 3.5. In (ii) the zero of potential corresponds to V(r,z) with r = 0.9 a, $z \to \infty$.

We want to compare the results given by eq. 3.8(a) for δ_n with the more rigorous expression :

$$\delta_n = \frac{1}{f_n} = \frac{1}{0.9\ a} \cdot \frac{1}{2}\ e \int_{z_n}^{z_{n+1}} \frac{(E_r - E_o)\, dz}{\frac{1}{2} m v^2}, \qquad \text{(iii)}$$

with $\frac{1}{2} mv^2 = e\left(V_{inj} - \Delta V(z)\right)$, $V_{inj} >> \Delta V(z)$.

With limits of integration $z = \pm \frac{1}{b}$, $z = \frac{1}{b}$, ∞ respectively for δ_1 and δ_2 one obtains :

$$\delta_1 = \frac{2I_1}{1.8\ a\ V_{inj}} \left[1 - \frac{\Delta V(o)}{V_{inj}} \left(\frac{4}{9} \exp(-.5) + \frac{2}{9} \exp 1 \right) \right], \qquad \text{(iv)}$$

$$\delta_2 = \frac{-I_1}{1.8\ a\ V_{inj}} \left(1 - \frac{\Delta V(o)}{V_{inj}} \frac{4}{9} \exp(-.5) \right), \qquad \text{(v)}$$

where higher order terms in $\Delta V/V_{inj}$ have been dropped and where

$$I_1 = \int_0^{1/b} (E_r - E_o)\, dz = - \int_{1/b}^{\infty} (E_r - E_o)\, dz = \frac{\Delta E(o)}{b} \exp(-1) \quad . \tag{vi}$$

The lens positions by equation 3.7 are $\bar{z}_1 = 0$ and $\bar{z}_2 = \pm \frac{2.68}{b}$ for δ_1 and δ_2 respectively.

Applying the method of equation 3.8 et seq. one obtains :

$$\bar{\delta}_1 = \frac{2I_1}{1.8\, a\, V_{inj}} \left(1 - \frac{\Delta V(o)}{V_{inj}}\right) , \tag{vii}$$

$$\bar{\delta}_2 = \frac{-I_1}{1.8\, a\, V_{inj}} \left(1 - \frac{\Delta V(o)}{V_{inj}} \exp(-1.34)\right) \quad . \tag{viii}$$

Substituting the numerical values

$$2\delta_2 + \delta_1 = \frac{-1.21\, I_1}{1.8\, a} \frac{\Delta V(o)}{V_{inj}^2} , \tag{ix}$$

$$2\bar{\delta}_2 + \bar{\delta}_1 = \frac{-1.48\, I_1}{1.8\, a} \frac{\Delta V(o)}{V_{inj}^2} \quad . \tag{x}$$

For this case (see Table 2) $2\bar{\delta}_2 + \bar{\delta}_1 \approx 5\bar{\delta}_1\bar{\delta}_2\ell$ so our simple numerical procedure overestimates the overall triplet strength by $\sim 18\%$. This compensates,to some extent, the error which arises via neglect of the change of charge density with ΔV.

APPENDIX 3

THERMAL EQUILIBRIUM MODEL

The charge density distribution of electrons in thermal equilibrium in a potential V(r) is obtained by integrating the Maxwell-Boltzmann distribution function over the velocity and is

$$\rho_e(r) = \rho_e(o) \exp\left[e\Big(V(r) - V(o) \Big) / k T_e \right] \quad \text{(i)}$$

where V_o is the potential on the axis.

The potential distribution in a beam of uniform proton density $\rho_i = \dfrac{I}{\pi a^2 \beta c}$ in the presence of electrons may then be calculated from Poisson's equation viz.

$$\frac{1}{r} \frac{d}{dr}\left(r \frac{dV}{dr} \right) = - \frac{\rho_i}{\varepsilon_o} \left[1 - f \exp\left[e\Big(V(r) - V(o) \Big) / k T_e \right] \right], \quad r < a$$

$$= \frac{\rho_i}{\varepsilon_o} f \exp\left[e \Big(V(r) - V(o) \Big) / k T_e \right] . \qquad r \geqslant a \qquad \text{(ii)}$$

where $f = \rho_e(o)/\rho_i$.

Putting $V'(r) = V(r) - V(o)$ and transforming to the dimensionless variables $\eta = V'(4\pi\varepsilon_o \beta c/I)$, $s = r/a$, we get

$$\frac{1}{s} \frac{d}{ds} \left(s \frac{d\eta}{ds} \right) = - 4 \left(1 - f\, e^{\eta/\xi} \right) \qquad s \leqslant 1 \quad ,$$

$$= 4 f\, e^{\eta/\xi} \qquad s \geqslant 1 \qquad \text{(iii)}$$

where $\xi = \dfrac{\beta k T_e}{30 I} = 2 \bar{\varepsilon} . \dfrac{\beta}{30 I}$ and $\bar{\varepsilon}$ is the electron mean energy.

A limiting condition on the value of the neutralisation factor f may be imposed by the following argument. Consider for simplicity a circular vacuum pipe of radius r_p inside which is contained the beam of radius a. The electrons are not restricted to the region inside the beam but may exist anywhere in the potential well inside the pipe provided their energy is sufficient. However the total number of electrons inside the pipe cannot exceed the total number of ions. If this were the case there would, according to Gauss' theorem, be an outward force on the electrons near the wall resulting in an immediately increased loss. Therefore the limiting value of f must be such that the gradient $d\eta/ds$ at the wall is zero. Using the above condition we may find a limiting solution of (iii) for the case of $T_e \to \infty$. For large T_e the electron contribution to the space charge becomes uniform over the whole of the beam pipe. The maximum neutralisation factor f may then be calculated simply since

$$\rho_e \cdot \pi r_p^2 = \rho_i \cdot \pi a^2 \qquad \text{(iv)}$$

or $f = a^2/r_p^2$.

For our standard case $a/r_p = 0.5$ a complete solution of (iii) gives

$$\eta' = \eta(s) - \eta(r) = 1.386 - 0.75\, s^2 \qquad s < 1$$
$$= 0.386 + 0.25\, s^2 - 2 \ln s, \quad 1 < s < 2$$

where η' is now the beam potential with respect to the wall. This limiting potential is shown dotted in Fig. 17a.

For the general case of finite T_e it is necessary to solve (iii) numerically searching for values of f which satisfy the boundary condition. Some typical results are shown on Fig. 17a. Fig. 17b shows the corresponding electron densities. We see that as the temperature (or ξ) increases, more and more electrons are able to occupy the space between the beam and pipe and therefore do not contribute to the neutralisation.

The following general conclusions may be drawn from this analysis :

1) The beam cannot be completely neutralised with electrons of finite energy. The degree of neutralisation attainable increases with decreasing electron temperature. This is because low energy electrons are mainly restricted to the region inside the beam where they contribute to the neutralisation.

2) A higher degree of neutralisation can be attained in small vacuum pipes than in large ones. This may be seen immediately for the limiting case of large T_e where the neutralisation factor varies inversely as the square of the pipe radius.

3) Particularly for small ξ the space charge forces acting on the proton beam are, although small, highly non-linear even though the proton density is uniform. Therefore on this model, an initially uniform beam cannot stay uniform when the space charge is neutralised.

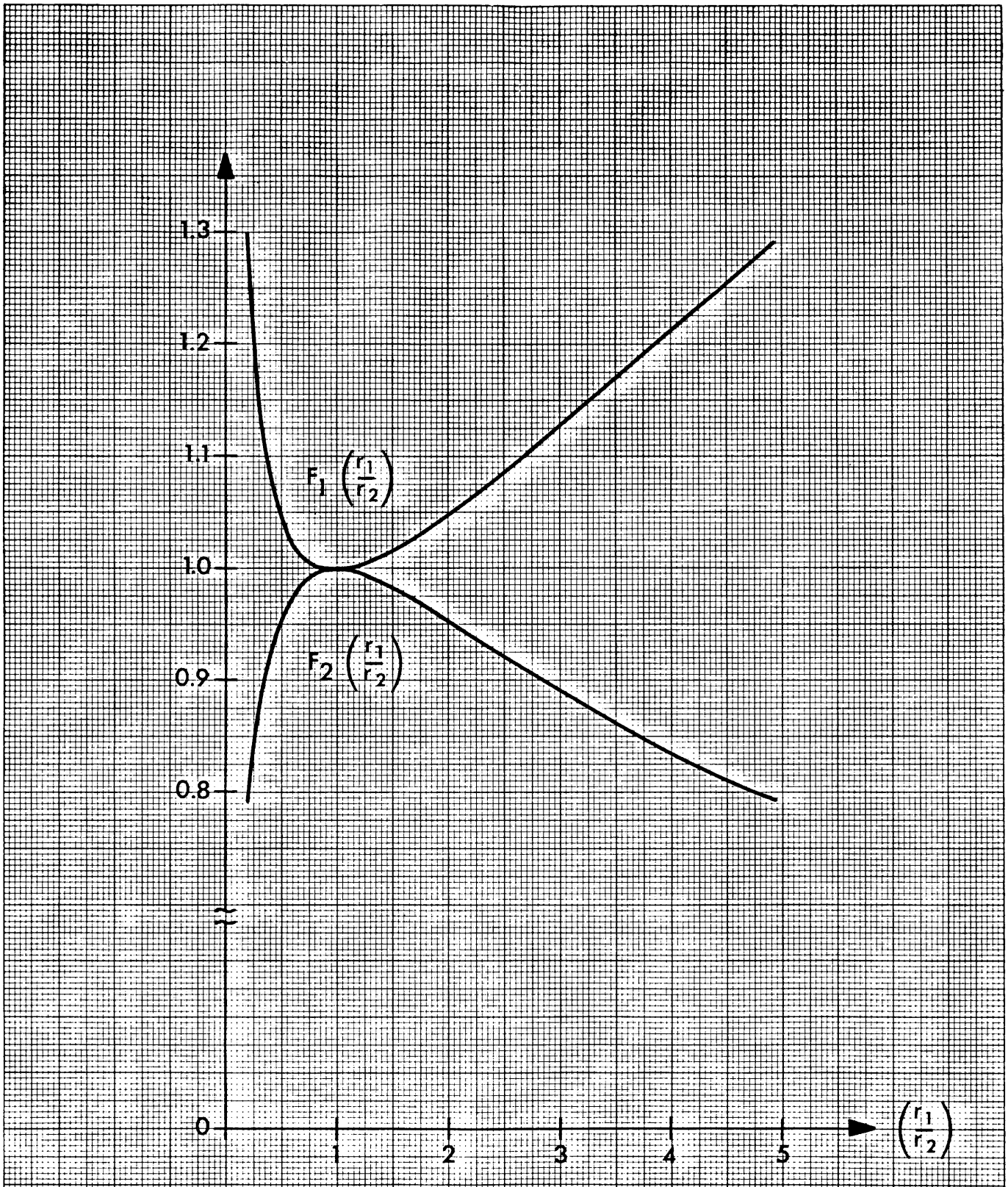

FIG. 1: Computed functions F_1, F_2 for optimised beam equations 2.9 and 2.10

105·2667-4 HPS 4158
E-913 20.8.71

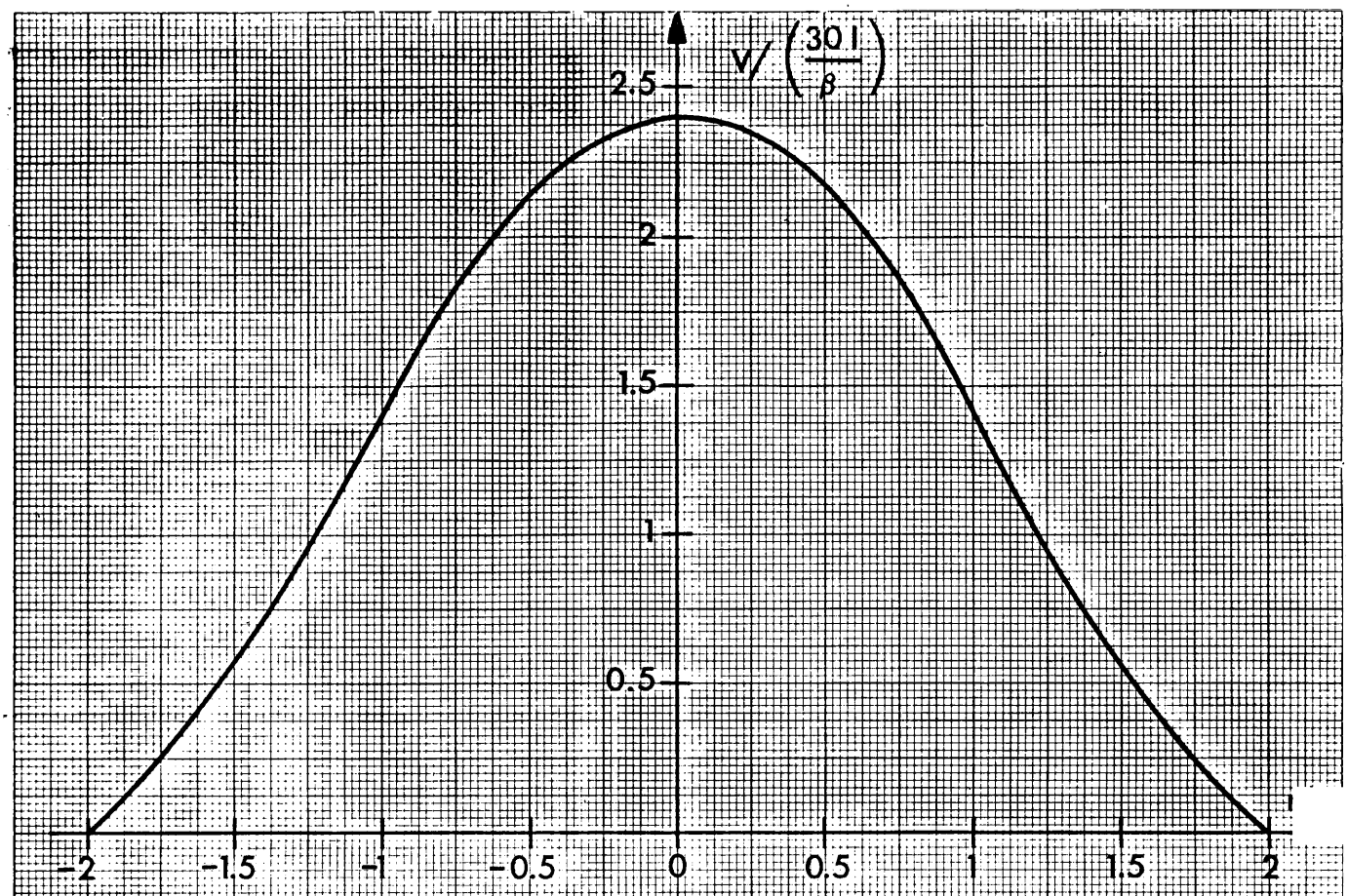

FIG. 2: Radial potential distribution for a uniform cylindrical beam radius s=r/a =1 in conducting pipe radius s=2

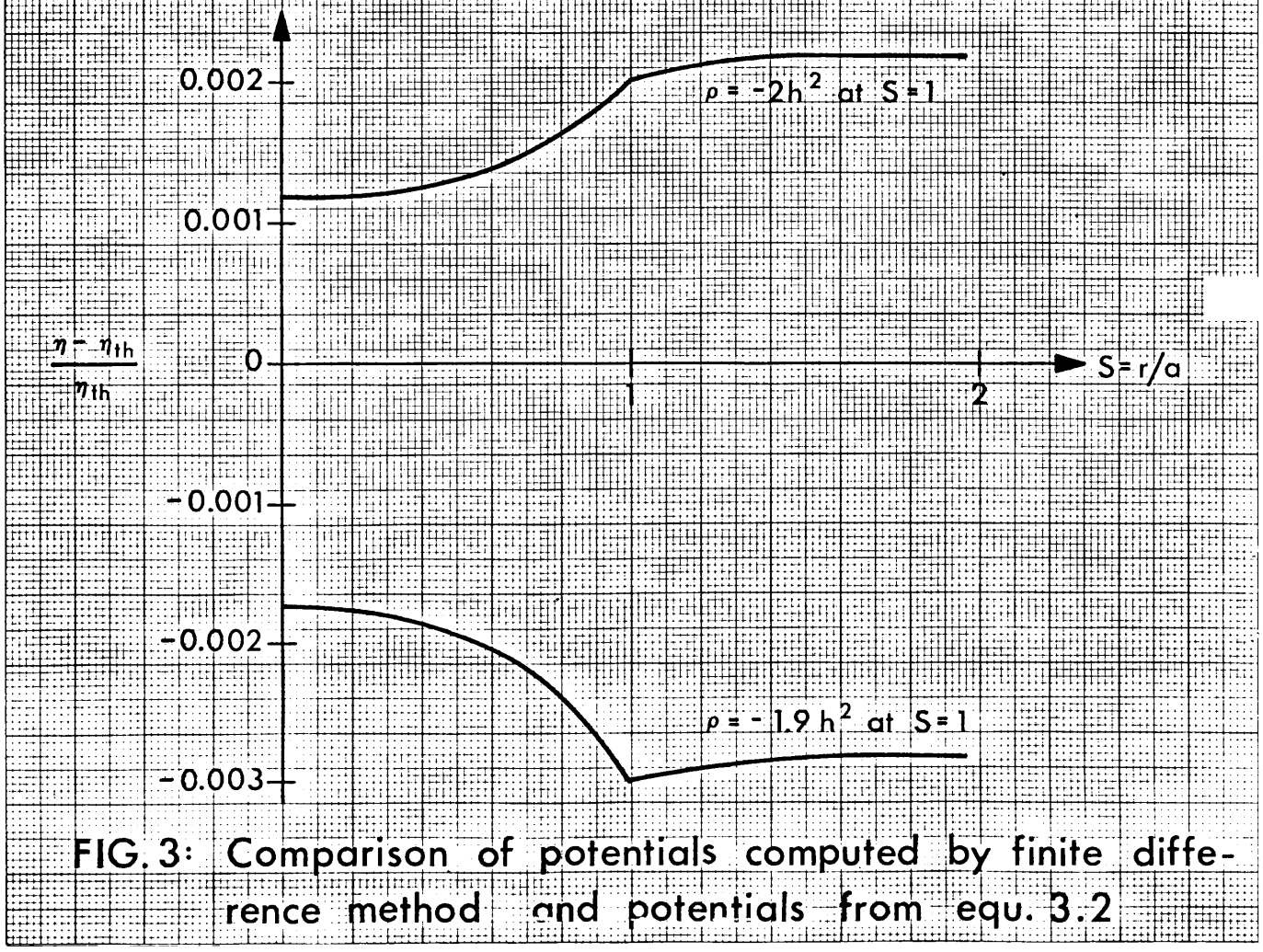

FIG. 3: Comparison of potentials computed by finite difference method and potentials from equ. 3.2

FABRICATION SUISSE
105-2668-4 MPS 4158
I-974 20.8.71 Lalonne

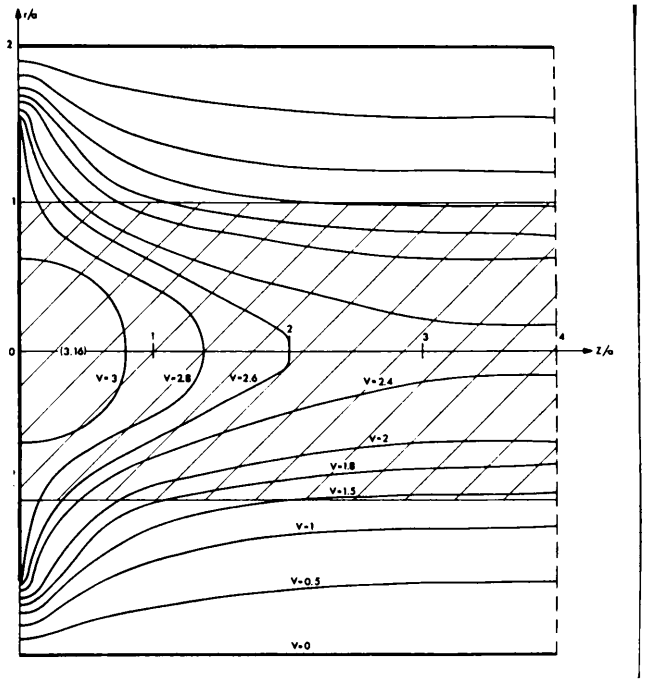

a) Bias Potential = + 3

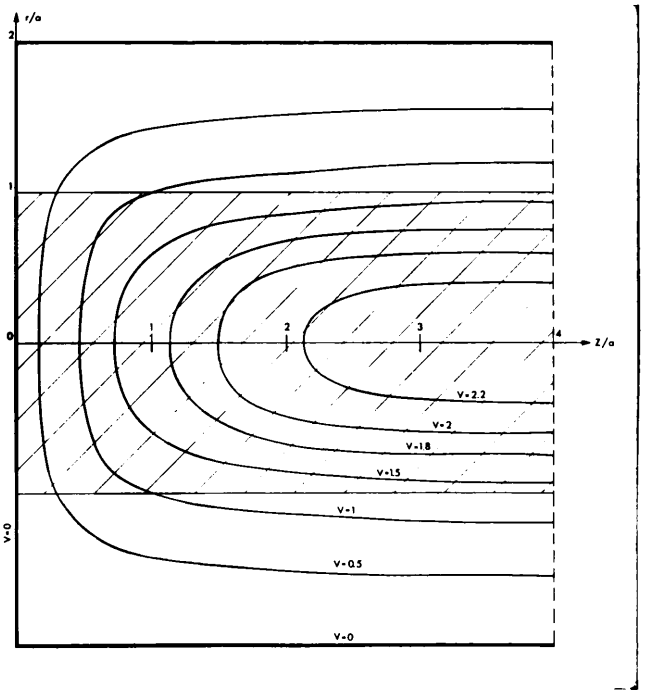

b) Bias Potential = 0

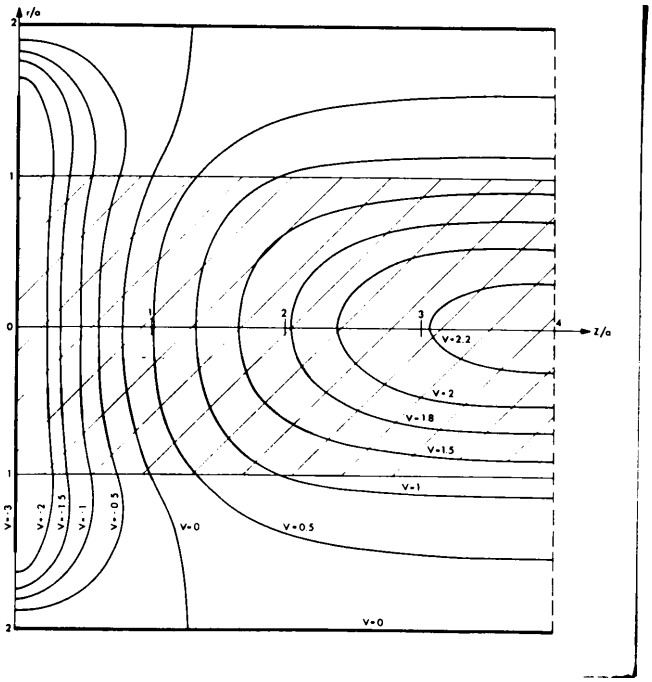

c) Bias Potential = - 3

Fig. 4 : Potential Distributions for Biased Stopping Plates.

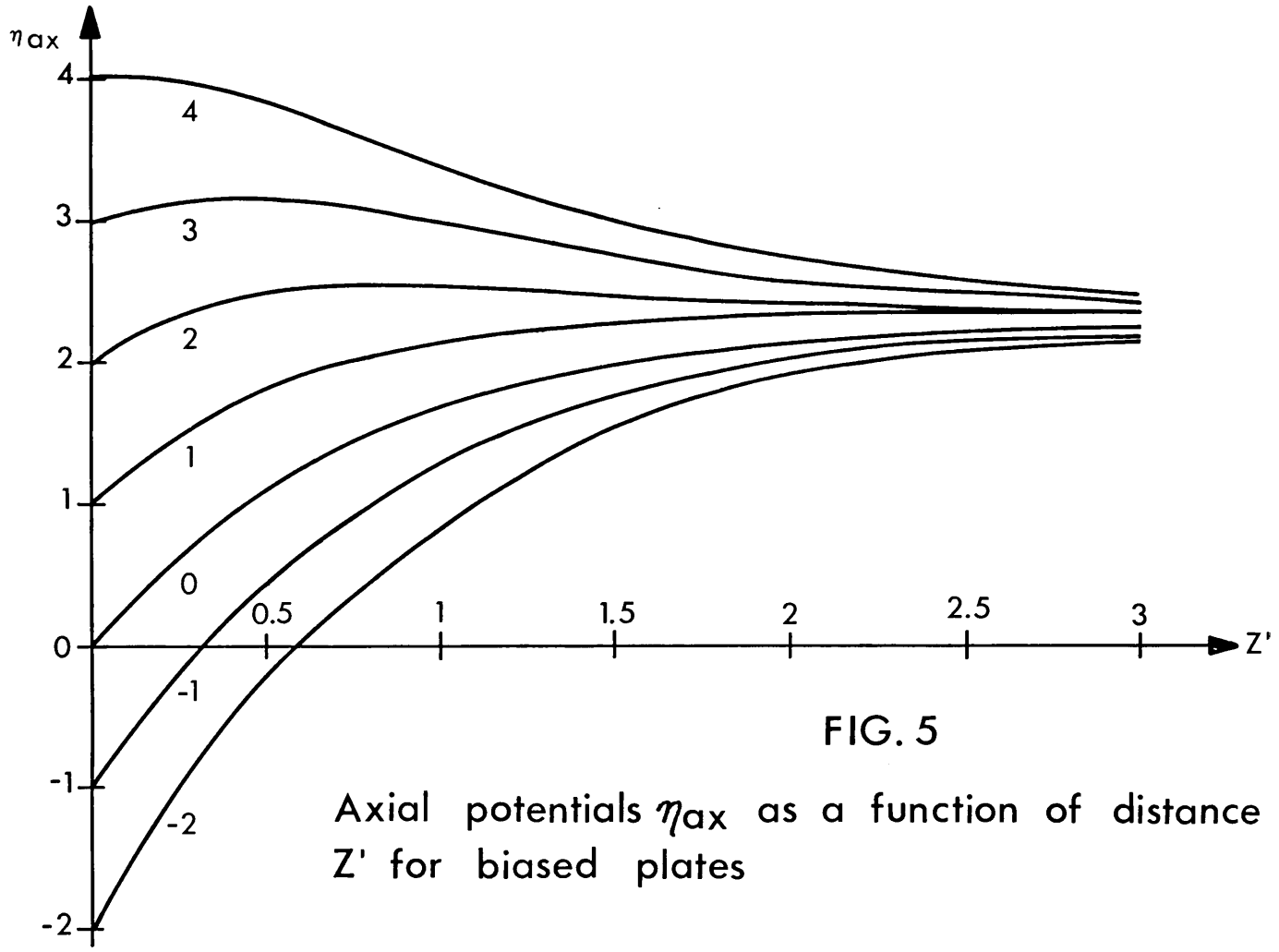

FIG. 5

Axial potentials η_{ax} as a function of distance Z' for biased plates

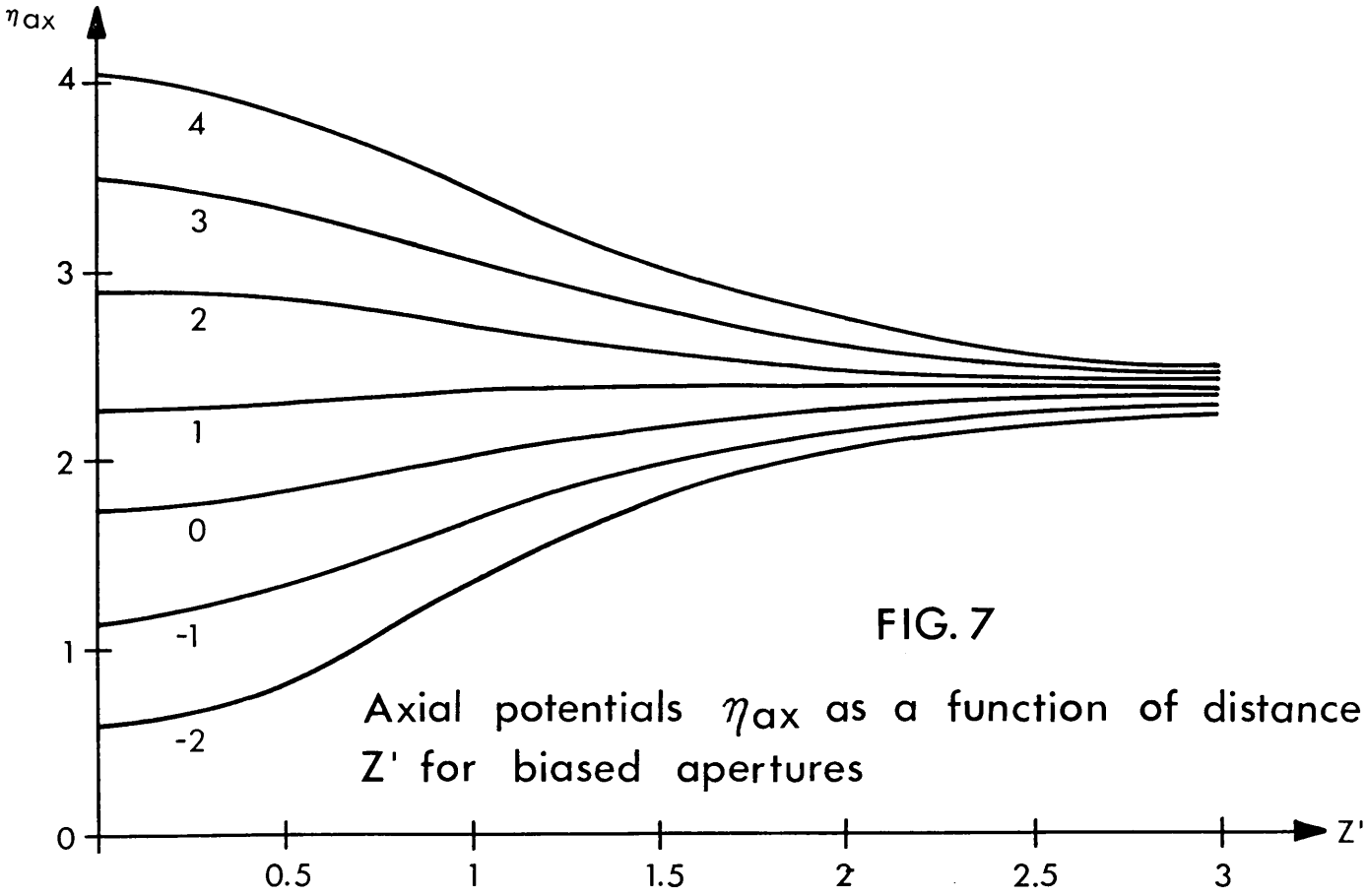

FIG. 7

Axial potentials η_{ax} as a function of distance Z' for biased apertures

105-2670-4 MPS 4158
I-976 20.8.71 Ladu

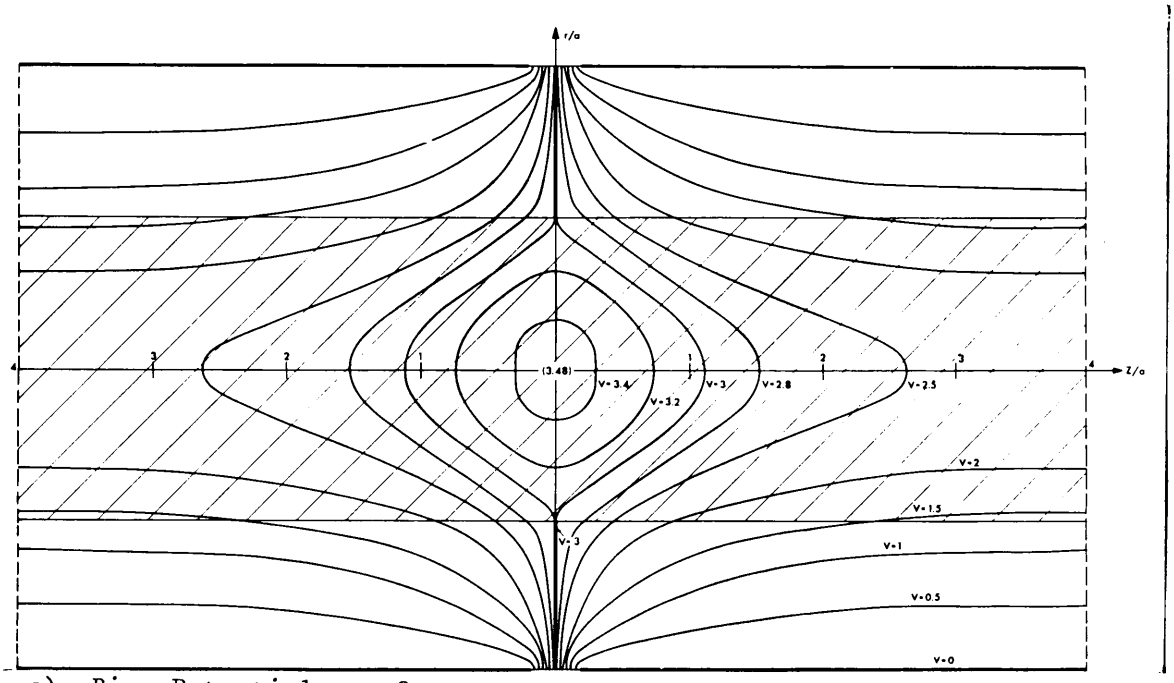

a) Bias Potential = + 3

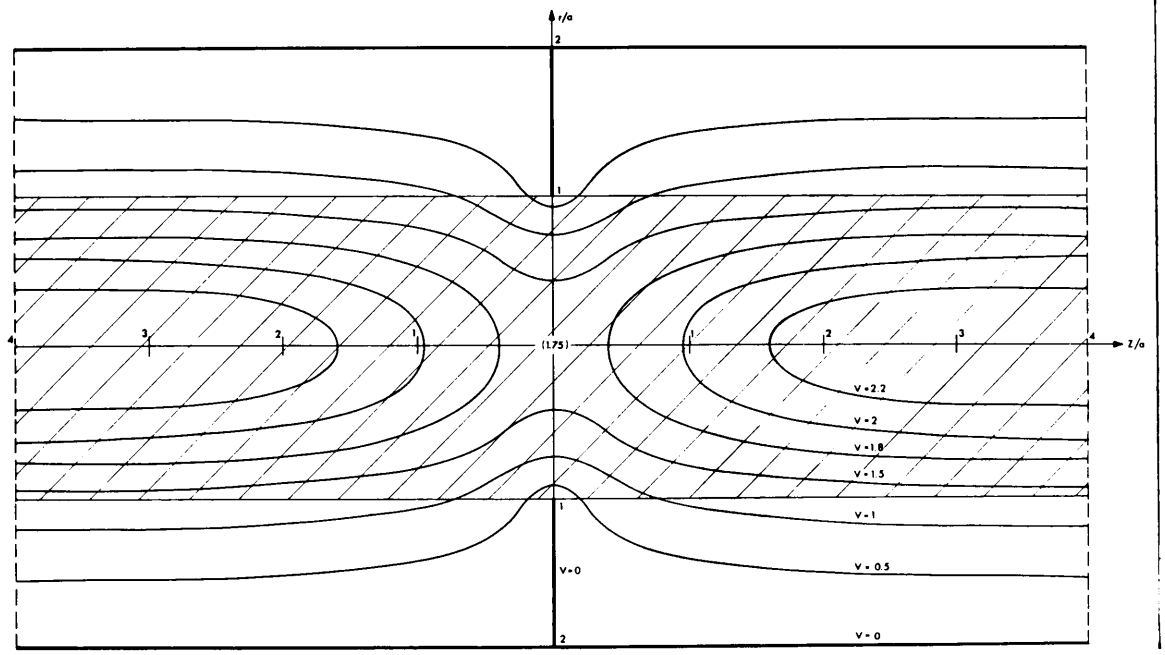

b) Bias Potential = 0

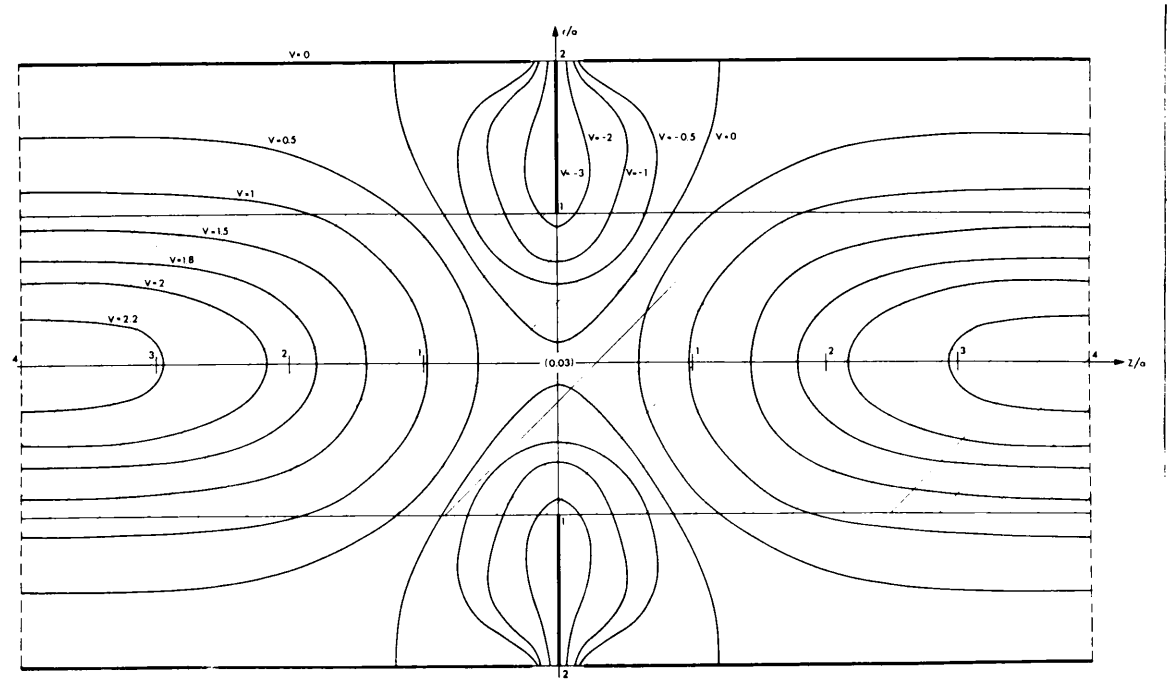

c) Bias Potential = - 3

Fig. 6 : Potential Distributions for Biased Apertures

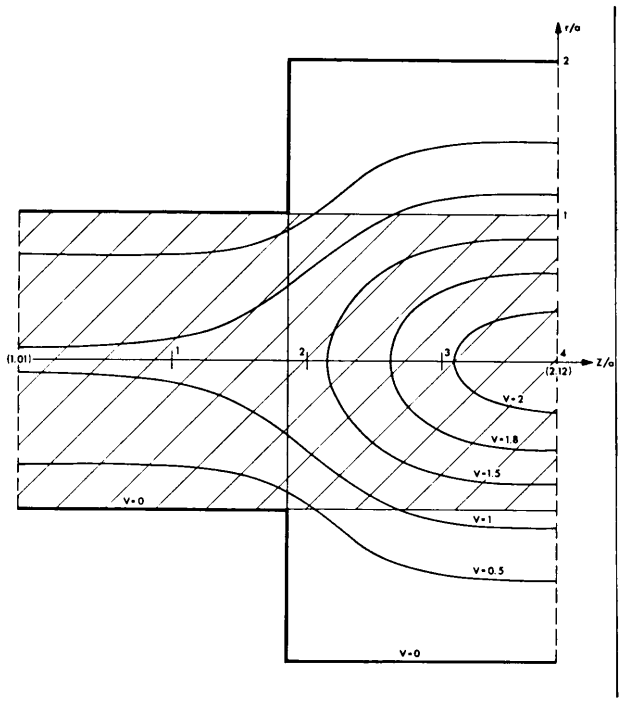

Fig. 8 : Potential Distribution when Pipe Diameter Changes

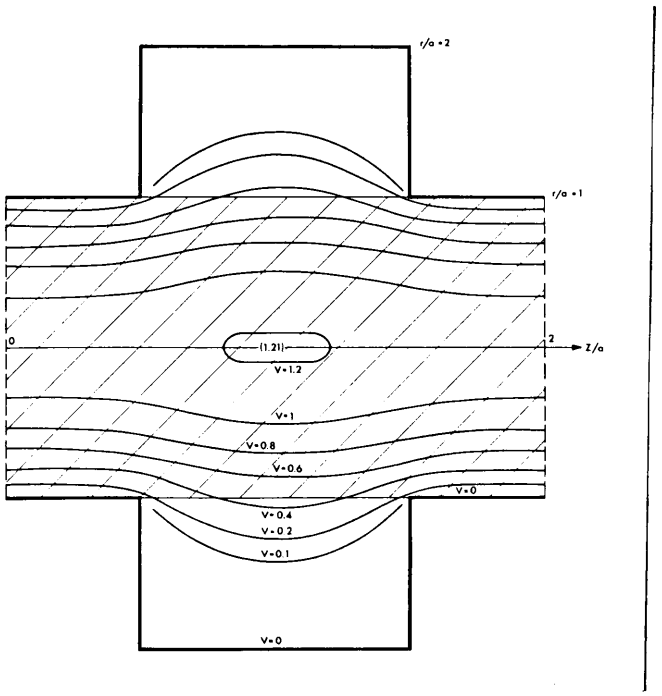

Fig. 9 : Potential Distribution for Simulated Drift-Tube/Gap Structure

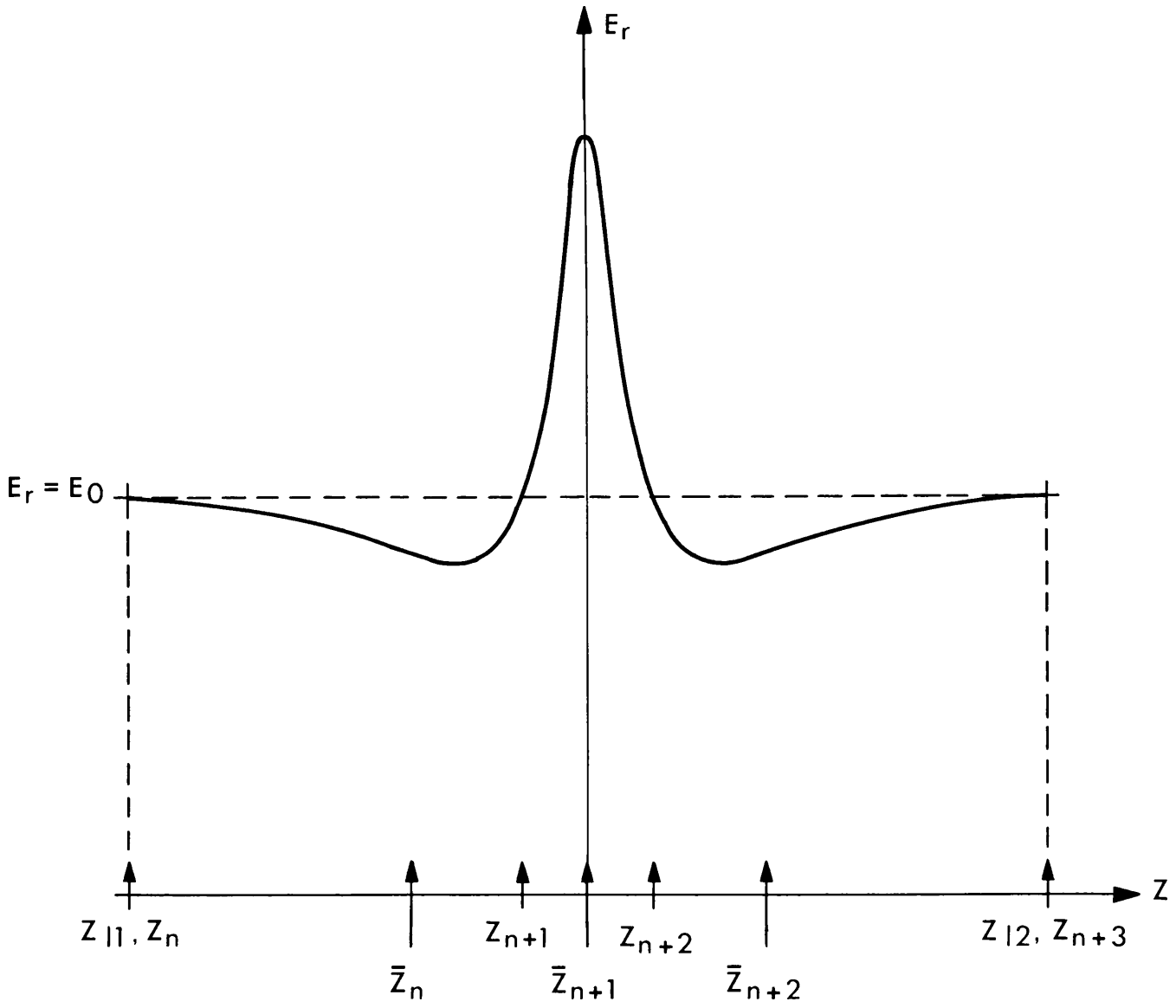

FIG. 10: Radial electric field E_r, at $S = r/a = 0.9$ for biased aperture; symbolism used in lens effect calculations

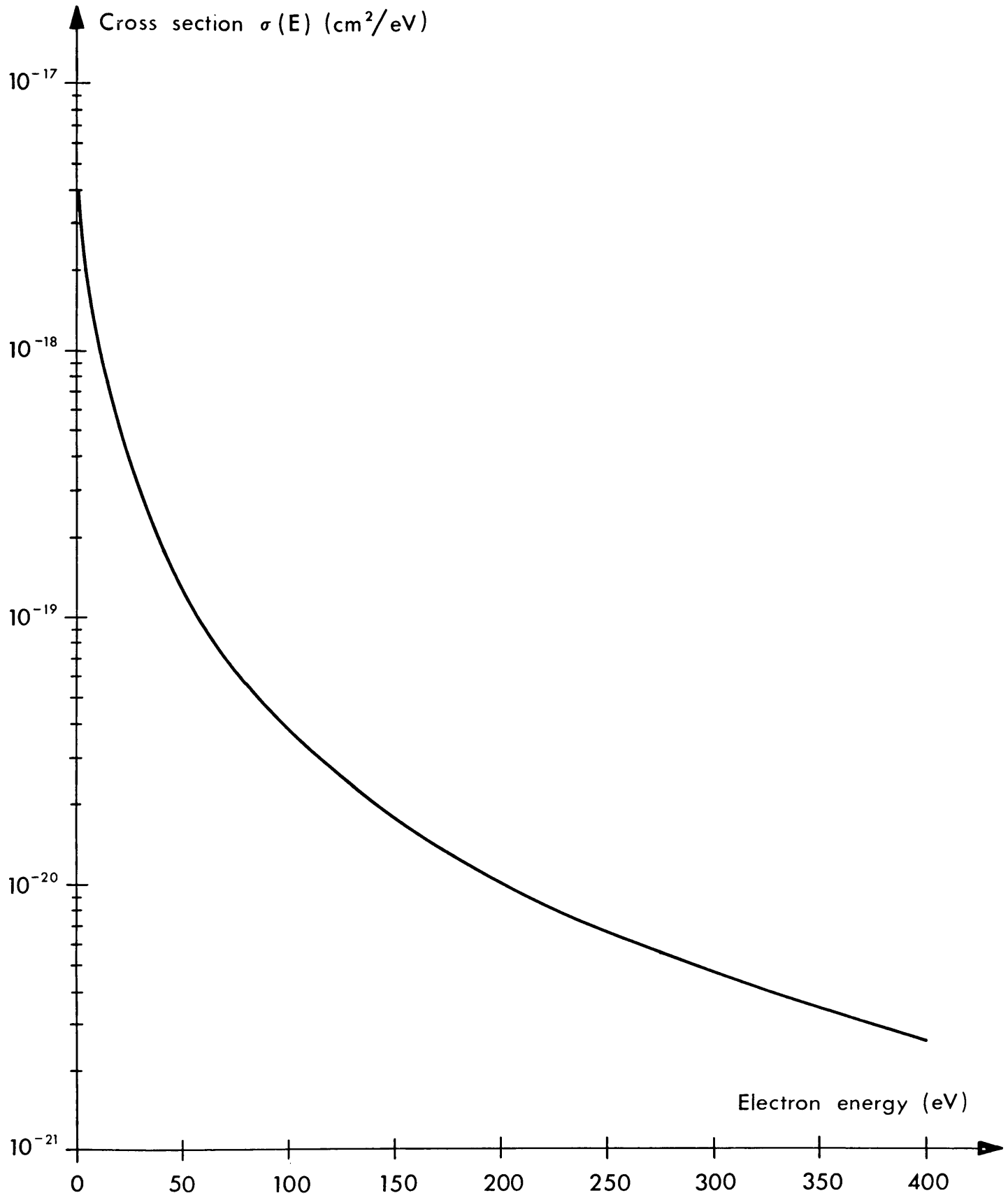

FIG. 11: Cross section for production of an electron with energy E for 500 keV protons in H_2

105-2671-4 MPS 4158
I-977 20.8.71 Lafour

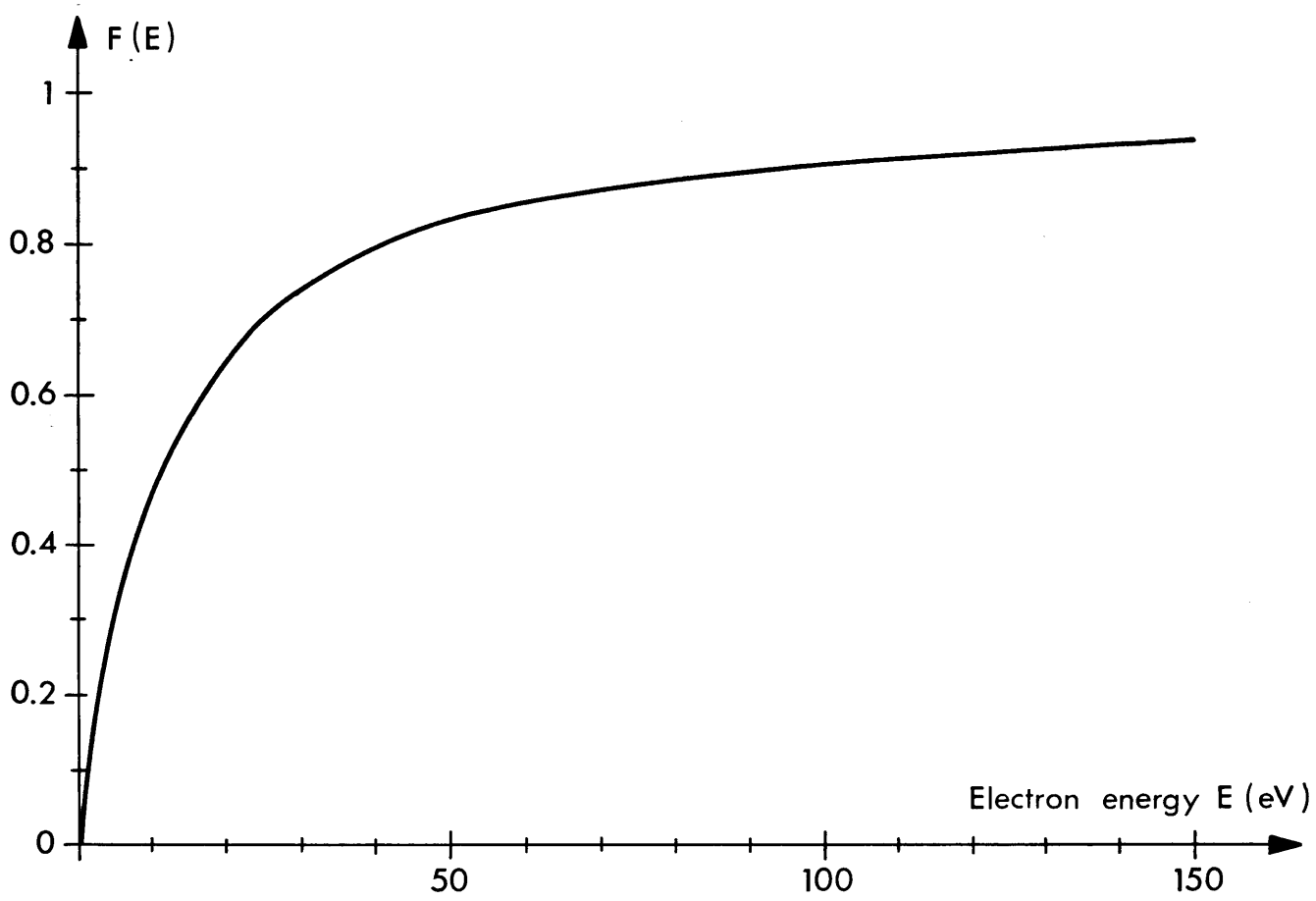

FIG. 12 : Fraction of electrons F(E) with energy less than E

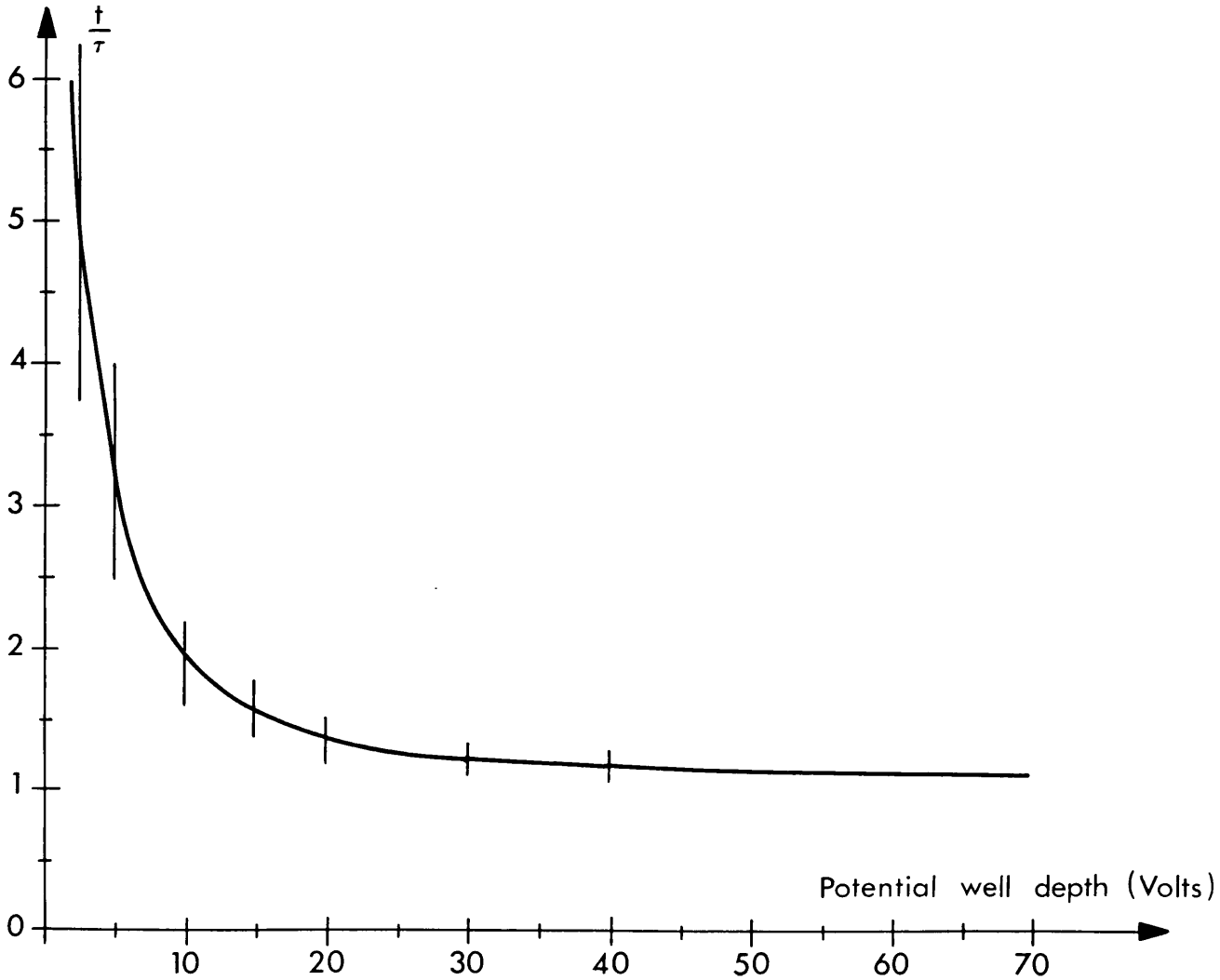

FIG. 13 : Neutralisation time t/τ as a function of well depth

105-2672-4 HPS 4158 I-978 20.8.71 Ad.

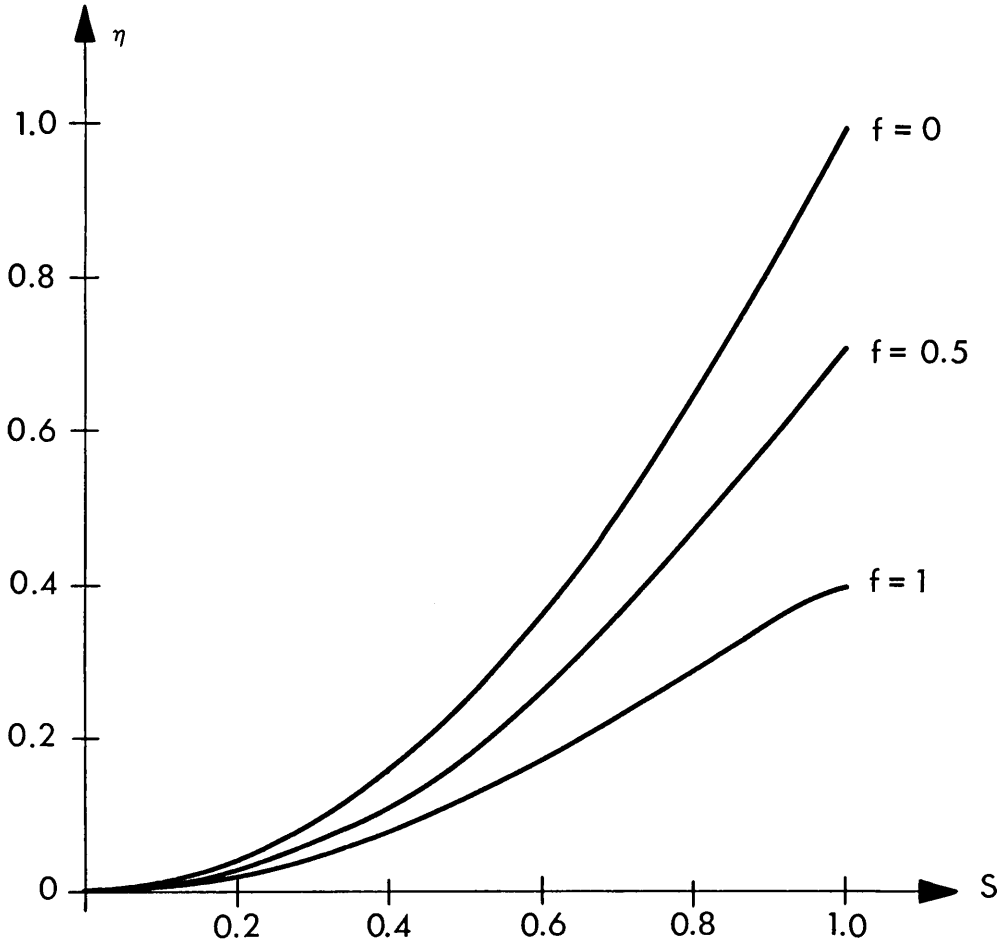

FIG. 14: Potential distribution for one dimensional beam with secondary electron neutralisation

105-2673-4 MPS 4158
I-979 20.8.71 Salorne

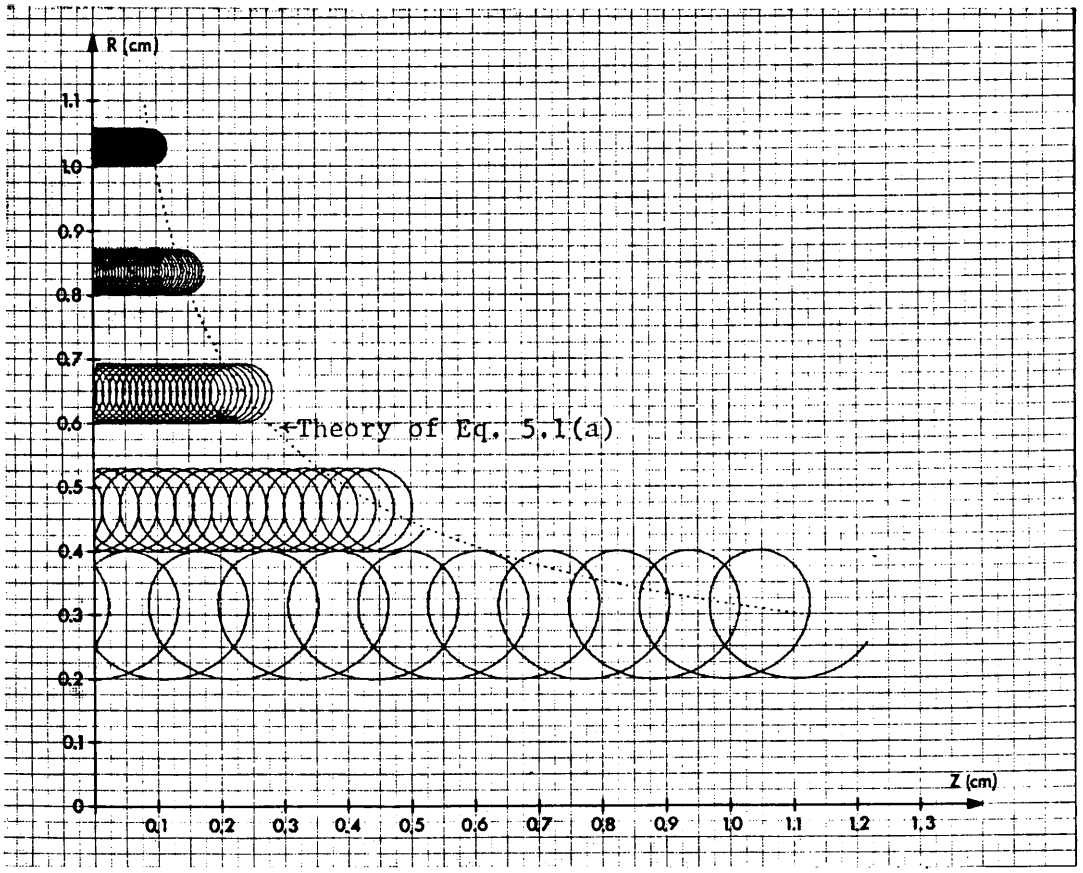

Fig. 15a : Electron Trajectories for 20 eV Electrons During 25 ns in a Magnetic Field Gradient 5 T m^{-1} (No Radial Electric Field).

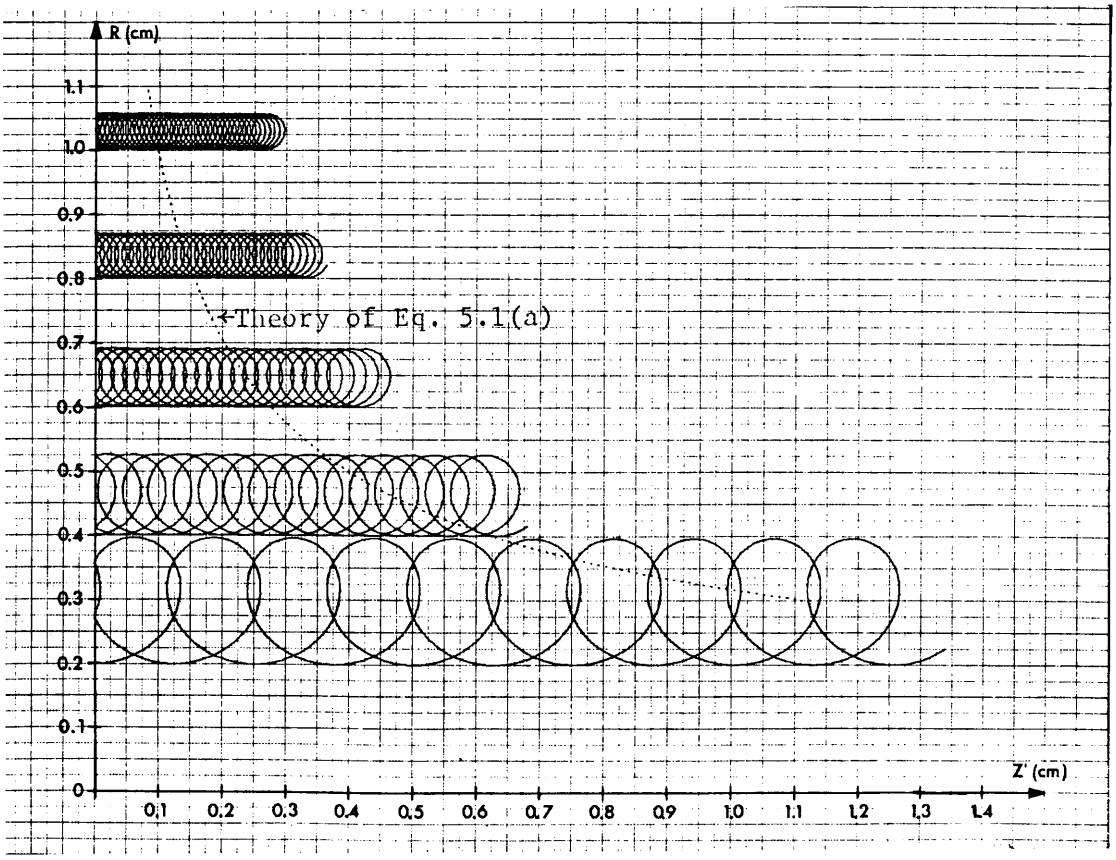

Fig. 15b : As 15a but with Radial Electric Field Gradient 3.6 kV m^{-1} (equivalent to 20 mA proton beam).

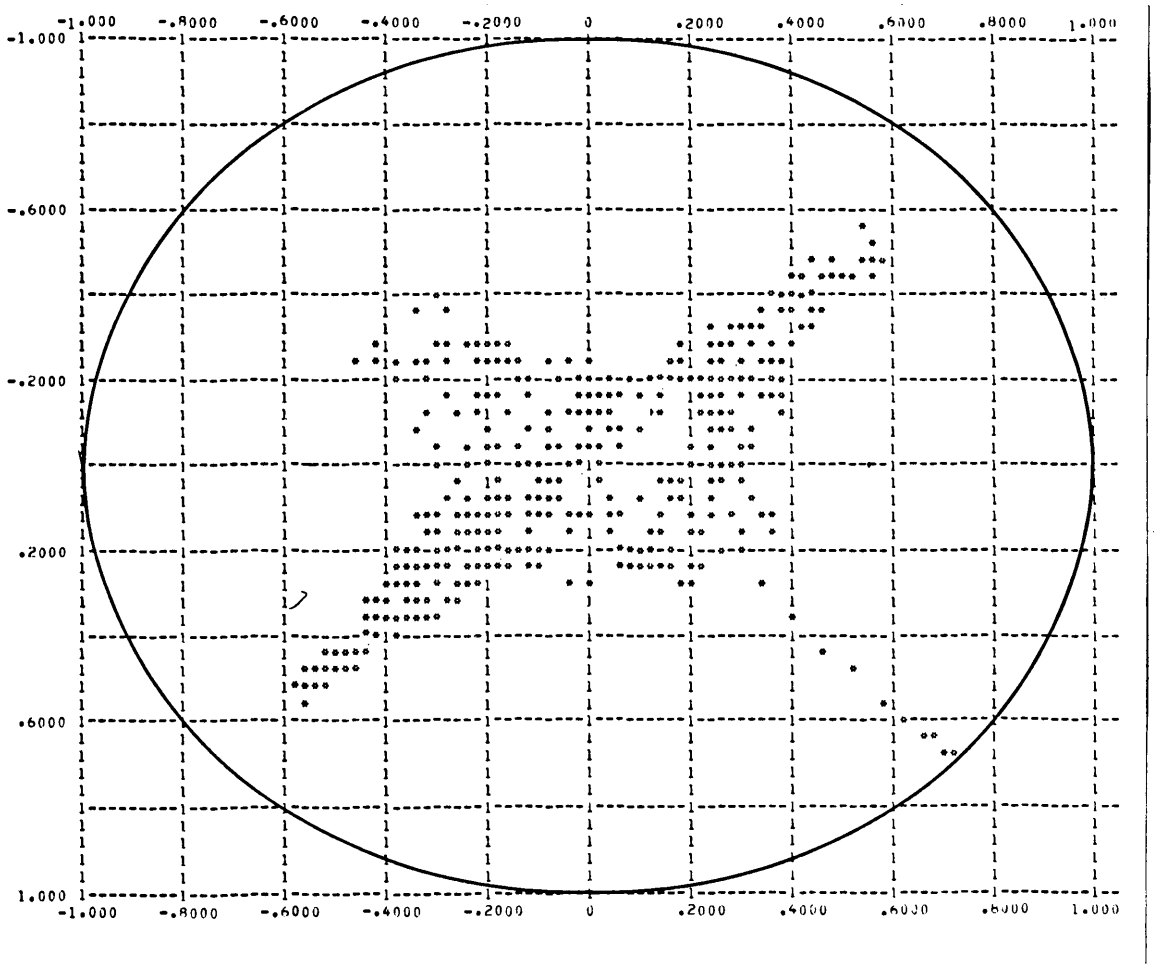

Fig. 16 : Typical Output of Orbit Calculation for an Electron Liberated from Drift Tube Wall at 1 eV. Quadrupole Field Gradient = 5 T/m, Proton Beam Current = 100 mA. Each Asterisk Represents a Point on the Trajectory.

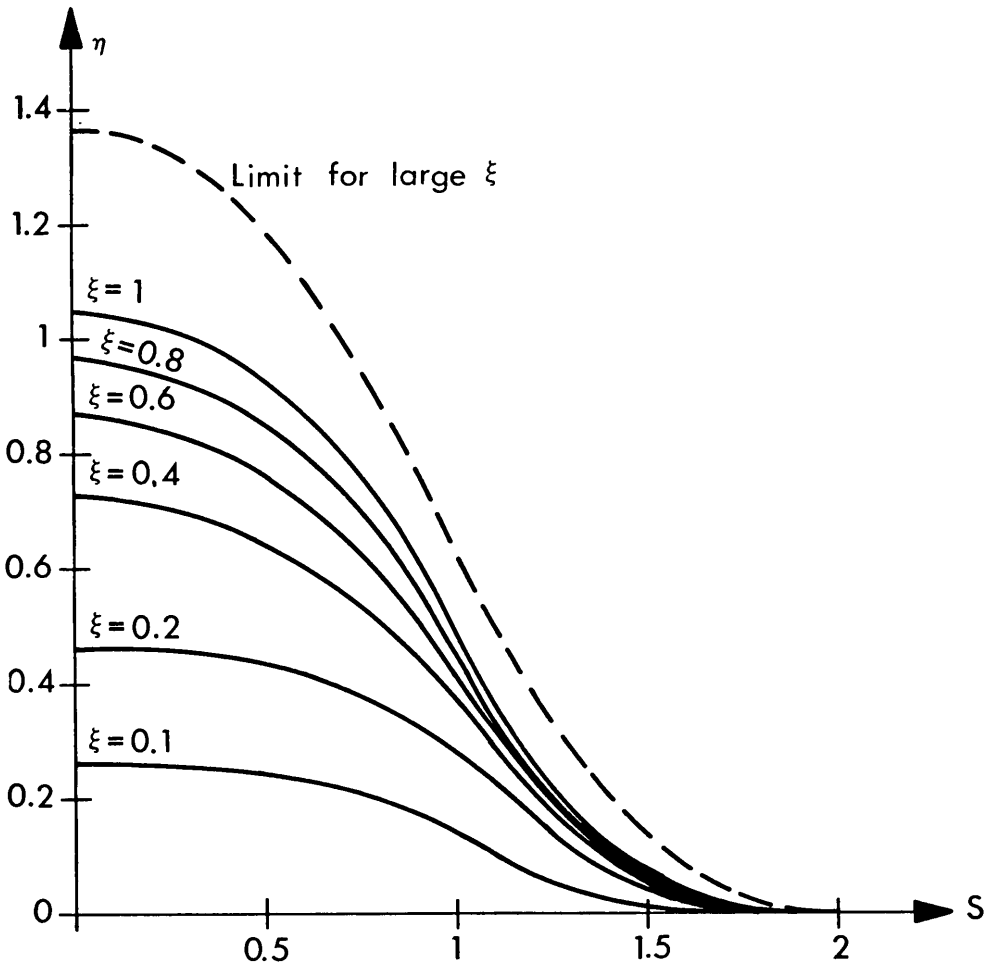

FIG. 17a: (App. 3) Potential distribution as a function of ξ for thermal equilibrium model

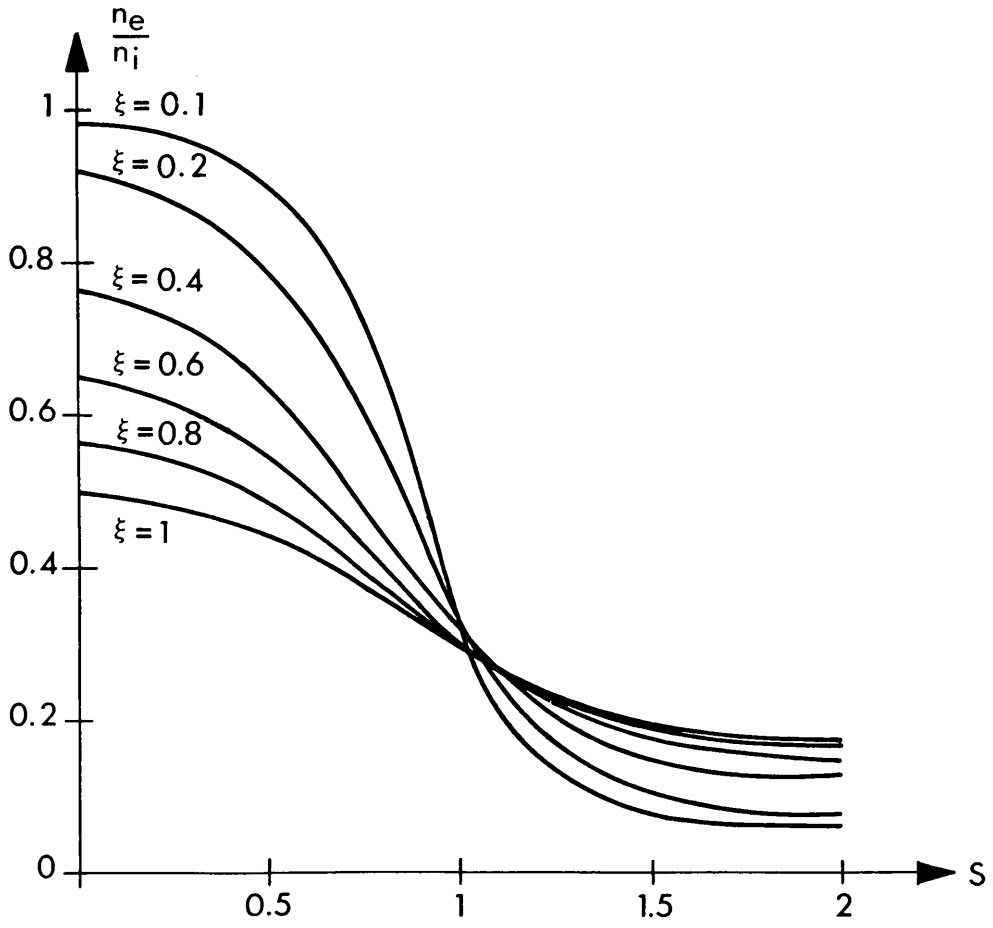

FIG. 17 b: (App. 3) Normalised electron density distribution

105-2674-4 MPS 4158
I-980 20.8.71 Jakeman